Human Rab small GTPase– and class V myosin–mediated membrane tethering in a chemically defined reconstitution system

Received for publication, August 9, 2017, and in revised form, September 21, 2017 Published, Papers in Press, September 22, 2017, DOI 10.1074/jbc.M117.811356

Motoki Inoshita and Joji Mima[1]

From the Institute for Protein Research, Osaka University, Suita, Osaka 565-0871, Japan

Edited by Henrik G. Dohlman

Membrane tethering is a fundamental process essential for the compartmental specificity of intracellular membrane trafficking in eukaryotic cells. Rab-family small GTPases and specific sets of Rab-interacting effector proteins, including coiled-coil tethering proteins and multisubunit tethering complexes, are reported to be responsible for membrane tethering. However, whether and how these key components directly and specifically tether subcellular membranes remains enigmatic. Using chemically defined proteoliposomal systems reconstituted with purified human Rab proteins and synthetic liposomal membranes to study the molecular basis of membrane tethering, we established here that Rab-family GTPases have a highly conserved function to directly mediate membrane tethering, even in the absence of any types of Rab effectors such as the so-called tethering proteins. Moreover, we demonstrate that membrane tethering mediated by endosomal Rab11a is drastically and selectively stimulated by its cognate Rab effectors, class V myosins (Myo5A and Myo5B), in a GTP-dependent manner. Of note, Myo5A and Myo5B exclusively recognized and cooperated with the membrane-anchored form of their cognate Rab11a to support membrane tethering mediated by *trans*-Rab assemblies on opposing membranes. Our findings support the novel concept that Rab-family proteins provide a *bona fide* membrane tether to physically and specifically link two distinct lipid bilayers of subcellular membranes. They further indicate that Rab-interacting effector proteins, including class V myosins, can regulate these Rab-mediated membrane-tethering reactions.

All eukaryotic cells, from yeast to human, deliver the correct sets of cargoes such as proteins and lipids to the appropriate cellular compartments, including a variety of subcellular organelles, the plasma membrane, and the extracellular space (1). These membrane-trafficking events are a fundamental and highly selective process in the eukaryotic endomembrane systems, ensuring that transport vesicles or other membrane-bounded carriers specifically recognize, physically bind to, and eventually fuse with the target membranes in a spatiotemporally regulated manner (1). A large body of prior genetic and biochemical studies have described miscellaneous key protein components functioning in eukaryotic membrane trafficking, which include SNAREs (soluble *N*-ethylmaleimide–sensitive factor attachment protein receptors) (2), SNARE-binding cofactors and chaperones such as Sec1/Munc18 proteins (3), Rab-family small GTPases (4, 5), and Rab-interacting proteins termed "Rab effectors" (6, 7). Membrane tethering mediated by Rab GTPases and Rab effectors is generally known to be the first contact between the transport carriers and the target membranes and thus an essential step in determining the specificity of intracellular membrane trafficking (8–10) followed by SNARE-mediated membrane fusion, which is another critical layer in conferring the fidelity of membrane trafficking (11–15). However, how Rab GTPases and Rab effectors work together to specifically drive membrane tethering still remains elusive (16–18), although recent biochemical reconstitution studies have begun to report the intrinsic membrane-tethering potency of specific Rab effectors (10, 19–23) and Rab GTPases (16, 18). In this study, to gain a deeper insight into the mechanisms of intracellular membrane tethering, we reconstituted membrane-tethering reactions in a chemically defined system from synthetic liposomes and purified human Rab GTPases and class V myosins as the cognate effectors of Rab11a, thereby comprehensively investigating their genuine functions in membrane tethering.

Results and discussion

Two prior studies on membrane tethering in a chemically defined reconstitution system explain that the tethering of synthetic liposomes can be triggered directly by several Rab-family GTPases themselves, which locate and function at the endosomal compartments in yeast (16) and human cells (18). This Rab-mediated tethering of liposomal membranes is an efficient and specific biochemical reaction, as we established by showing that membrane-anchored human Rab5a rapidly induces the formation of massive liposome clusters and also that the tethering activity of Rab5a can be strictly and reversibly controlled by the membrane attachment and detachment of Rab proteins on both opposing membranes (18). Intriguingly, Rab5a-mediated membrane tethering was not blocked by the addition of a large excess of soluble Rab5a proteins lacking a membrane

This study was supported in part by the Program to Disseminate Tenure Tracking System from the Ministry of Education, Culture, Sports, Science, and Technology, Japan (MEXT) and by grants-in-aid for scientific research from MEXT (to J. M.). The authors declare that they have no conflicts of interest with the contents of this article.

This article contains supplemental Figs. S1–S3.

[1] To whom correspondence should be addressed: Institute for Protein Research, Osaka University, 3-2 Yamadaoka, Suita, Osaka 565-0871, Japan. Tel.: 81-6-6879-4326; Fax: 81-6-6879-4329; E-mail: joji.mima@protein.osaka-u.ac.jp.

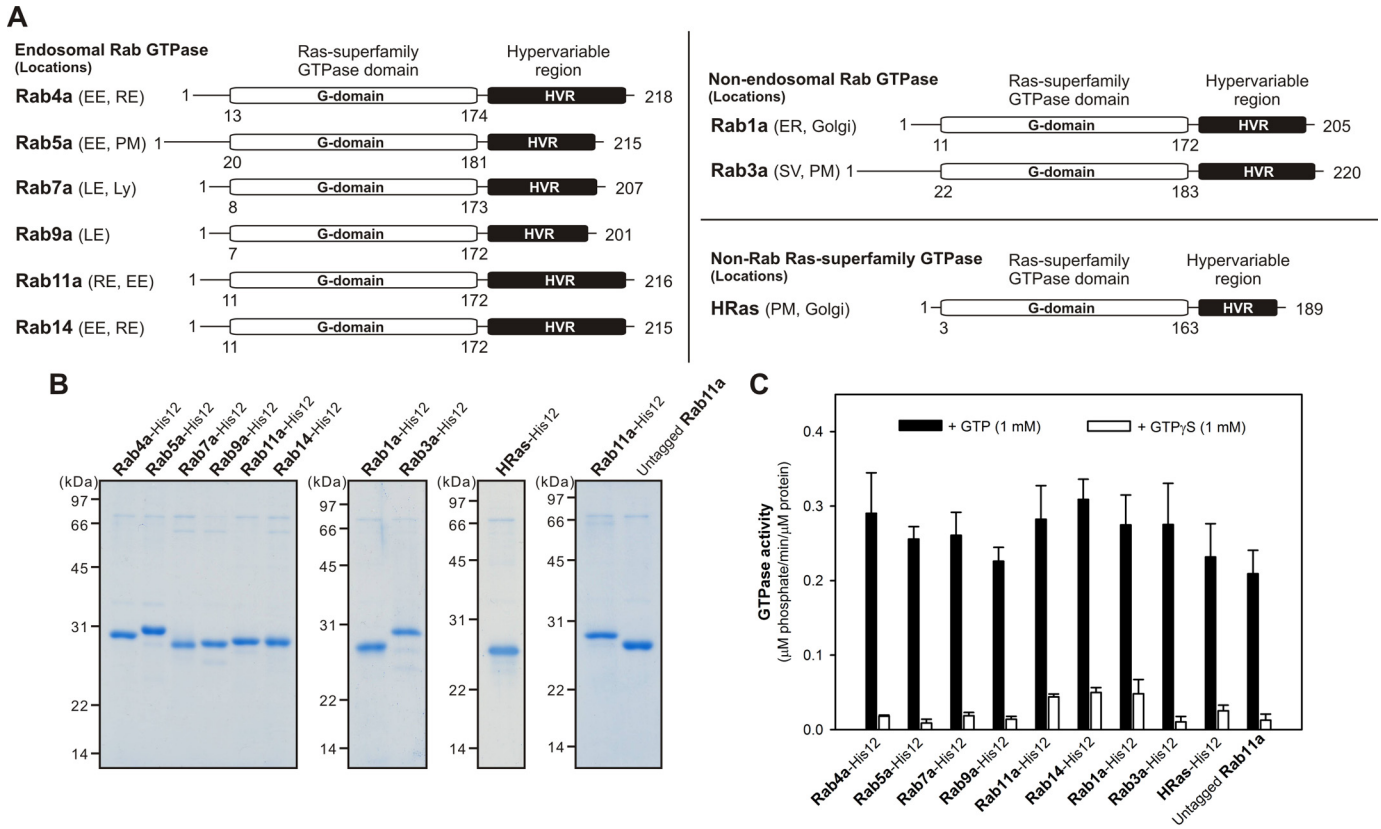

Figure 1. Purification of human Rab GTPases used in this reconstitution study. *A*, schematic representation of the endosomal Rabs (Rab4a, Rab5a, Rab7a, Rab9a, Rab11a, and Rab14), non-endosomal Rabs (Rab1a and Rab3a), and HRas GTPase in humans showing their amino acid residues, domains (Ras-superfamily GTPase domains and hypervariable regions), and intracellular locations, which include early endosome (*EE*), recycling endosome (*RE*), plasma membrane (*PM*), late endosome (*LE*), lysosome (*Ly*), ER, Golgi, and secretory vesicle (*SV*). *B*, Coomassie Blue-stained gels of purified recombinant proteins of the C-terminally His_{12}-tagged endosomal Rab, non-endosomal Rab, and HRas GTPases and the untagged form of Rab11a used in this study. *C*, intrinsic GTP hydrolysis activities of purified Rab proteins. Purified Rab-His_{12}, HRas-His_{12}, and untagged Rab11a proteins (2 μM) were incubated at 30 °C for 1 h in RB150 containing $MgCl_2$ (6 mM), DTT (1 mM), and GTP (1 mM) or GTPγS (1 mM) for the control followed by an assay of the released free phosphate molecules using a malachite green-based reagent.

anchor at their C termini (18), indicating that this membrane-tethering process cannot be explained simply by protein dimerization and protein-protein interactions in solution. Thus, our previous results strongly suggest a critical requirement of *trans*-Rab-Rab interactions on two distinctly opposing membranes for a reversible membrane-tethering event (18).

In the current reconstitution study, to further comprehensively investigate the inherent membrane-tethering potency of Rab-family GTPases in human, we purified and tested the six representative Rab GTPases functioning in the endocytic pathways (Rab4a, Rab5a, Rab7a, Rab9a, Rab11a, and Rab14) (7), for typical non-endosomal Rabs, Rab1a in ER[2]-to-Golgi traffic and Rab3a in exocytosis (4, 5), and also HRas for the control protein of a non-Rab small GTPase in the Ras superfamily (24) (Fig. 1*A*). All of the Rab-family and HRas GTPase proteins were purified as their full-length forms, consisting of the N-terminal non-conserved flexible segments (5–30 residues), the conserved globular Ras-superfamily GTPase domains in the middle (160–170 residues), and the so-called C-terminal hypervariable region (HVR) domains (20–50 residues) (24) (Fig. 1, *A* and *B*). In addition to the full-length amino acid sequences of the native proteins, to mimic membrane binding and anchoring of native Rab and HRas proteins through their isoprenyl or palmitoyl lipid anchors at the C terminus (5, 24), these recombinant Rab and HRas proteins used here were further artificially modified with a C-terminal polyhistidine tag (His_{12}), which can be stably associated with synthetic liposomal membranes bearing a DOGS-NTA lipid (1,2-dioleoyl-*sn*-glycero-3-{[*N*-(5-amino-1-carboxypentyl)iminodiacetic acid]-succinyl}) (Figs. 1*B* and 2*A*). We employed GTPase activity assays for all of the purified Rab-His_{12} and HRas-His_{12} proteins, indicating that they retained the comparable intrinsic GTPase activities, which specifically converted GTP to GDP and a free phosphate (Fig. 1*C*). Thus, this establishes that purified Rab- His_{12} and HRas-His_{12} proteins from the current preparations are all well-folded and functionally active in solution (Fig. 1*C*).

Dissecting the membrane-tethering potency of human Rab GTPases in a chemically defined reconstitution system

The intrinsic potency of human Rab GTPases to directly drive membrane tethering was thoroughly evaluated by the kinetics of the increase in turbidity of liposome suspensions in the presence of Rab proteins, which can be monitored by measuring absorbance at 400 nm (Figs. 2 and 3) (18, 25–27). Rab-

[2] The abbreviations used are: ER, endoplasmic reticulum; DOGS-NTA, 1,2-dioleoyl-*sn*-glycero-3-{[*N*-(5-amino-1-carboxypentyl)iminodiacetic acid]-succinyl}); PE, phosphatidylethanolamine; PI, phosphatidylinositol; Rh, rhodamine; Myo5, class V myosin; GTD, globular tail domain; GTPγS, guanosine 5′-*O*-(thiotriphosphate); HRV, human rhinovirus; FL, fluorescein; TRITC, tetramethylrhodamine isothiocyanate.

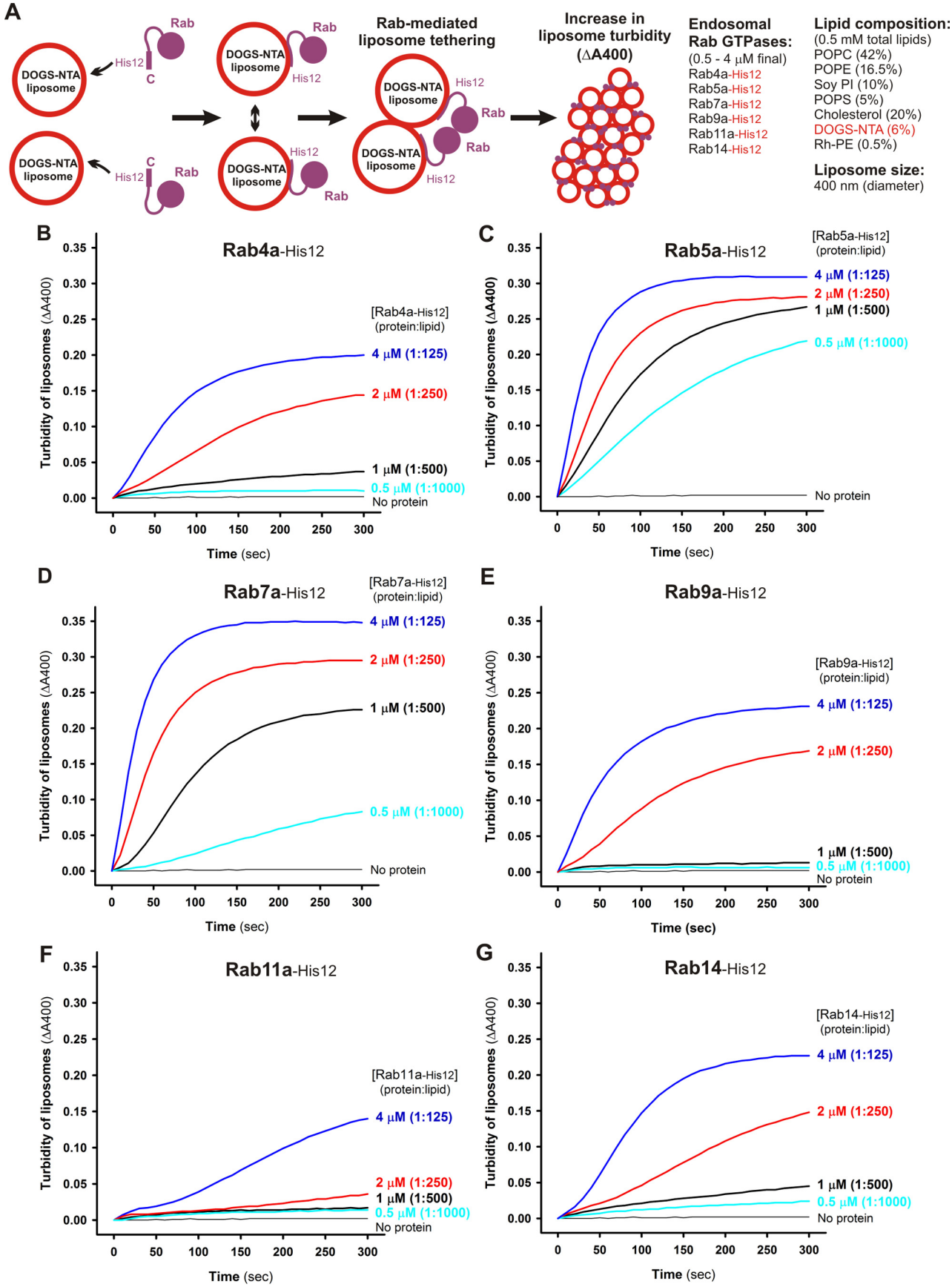
A
DOGS-NTA liposome
His12
C
Rab
Rab-mediated liposome tethering
Increase in liposome turbidity (ΔA400)
Endosomal Rab GTPases:
(0.5 - 4 μM final)
Rab4a-His12
Rab5a-His12
Rab7a-His12
Rab9a-His12
Rab11a-His12
Rab14-His12
Lipid composition:
(0.5 mM total lipids)
POPC (42%)
POPE (16.5%)
Soy PI (10%)
POPS (5%)
Cholesterol (20%)
DOGS-NTA (6%)
Rh-PE (0.5%)
Liposome size:
400 nm (diameter)
B
Rab4a-His12
[Rab4a-His12] (protein:lipid)
4 μM (1:125)
2 μM (1:250)
1 μM (1:500)
0.5 μM (1:1000)
No protein
C
Rab5a-His12
[Rab5a-His12] (protein:lipid)
D
Rab7a-His12
[Rab7a-His12] (protein:lipid)
E
Rab9a-His12
[Rab9a-His12] (protein:lipid)
F
Rab11a-His12
[Rab11a-His12] (protein:lipid)
G
Rab14-His12
[Rab14-His12] (protein:lipid)
Turbidity of liposomes (ΔA400)
Time (sec)

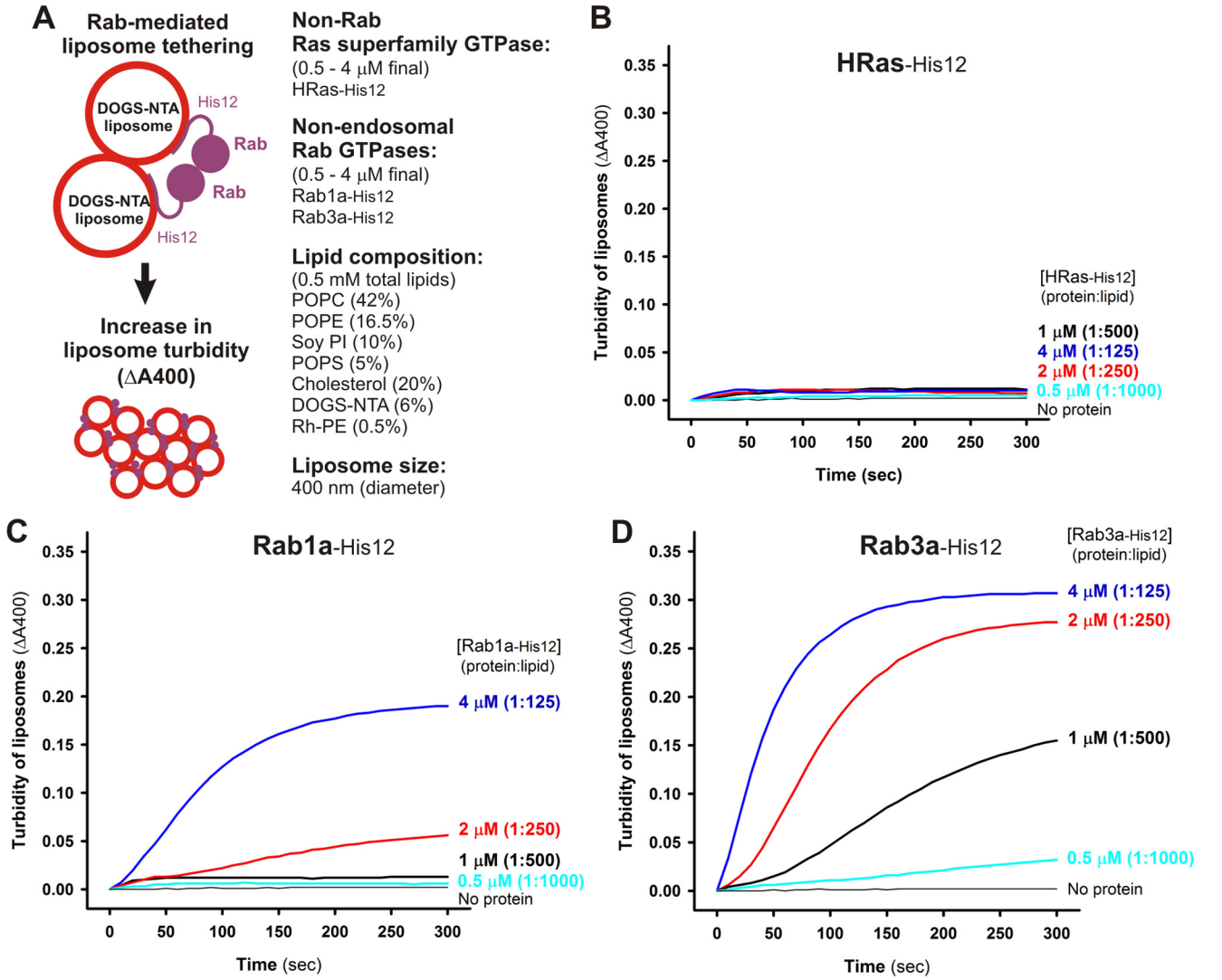

Figure 3. Non-endosomal Rab GTPases have the inherent potency to specifically mediate membrane tethering. *A*, schematic representation of liposome turbidity assays for the non-Rab Ras-superfamily GTPase, HRas, and non-endosomal Rab GTPases, Rab1a in ER-Golgi traffic and Rab3a in exocytosis (shown in *B–D*). *B–D*, liposome turbidity assays were employed as described in the legend for Fig. 2, *B–G*, with HRas-His$_{12}$ (*B*), Rab1a-His$_{12}$ (*C*), and Rab3a-His$_{12}$ (*D*) proteins (each at 0.5–4 μM in final) and physiological mimic synthetic liposomes (0.5 mM total lipids in final). The protein-to-lipid molar ratios used are indicated.

anchored liposomes were generated with purified Rab-His$_{12}$ proteins and synthetic liposomes (400 nm in diameter) bearing a DOGS-NTA lipid and five major lipid species of phosphatidylcholine (PC), phosphatidylethanolamine (PE), phosphatidylinositol (PI), phosphatidylserine (PS), and cholesterol, roughly recapitulating the lipid composition of subcellular organelle membranes in mammalian cells (Fig. 2*A*) (28). Because the efficacy of Rab-mediated liposome tethering was dependent on the lipid composition, liposome size, and total lipid concentration (supplemental Fig. S1) (18), we optimized the experimental conditions of liposome suspensions used for turbidity assays (Fig. 2*A*). With respect to Rab proteins tested in the tethering assays, as prior studies using the chemically defined reconstitution system report the intrinsic tethering activity of several Rab proteins in the endocytic trafficking pathways of yeast (the Rab5 ortholog Vps21p) (16) and human cells (Rab5a and Rab7a) (18), first we selected six representative endosomal Rabs (Rab4a, Rab5a, Rab7a, Rab9a, Rab11a, and Rab14) in humans for comprehensive analysis of the tethering potency of Rab-family GTPases (Fig. 2, *B–G*). By applying the liposome turbidity assay to the six Rab proteins at variable concentrations ranging from 0.5 to 4 μM toward 0.5 mM total lipids in the reactions (Fig. 2*A*), a rapid increase in liposome turbidity was triggered specifically either by Rab5a or Rab7a, even at low protein concentrations (0.5–1.0 μM, corresponding to the protein-to-lipid molar ratios of 1:1000 –1:500) (Fig. 2, *C* and *D*). This established

Figure 2. Endosomal Rab GTPases directly initiate membrane tethering by themselves in a chemically defined reconstitution system. *A*, schematic representation of liposome turbidity assays for testing Rab-mediated liposome tethering (shown in *B–G*). *B–G*, endosomal Rab-His$_{12}$ proteins (each at 0.5–4 μM), Rab4a-His$_{12}$ (*B*), Rab5a-His$_{12}$ (*C*), Rab7a-His$_{12}$ (*D*), Rab9a-His$_{12}$ (*E*), Rab11a-His$_{12}$ (*F*), and Rab14-His$_{12}$ (*G*), were incubated with synthetic liposomes bearing physiological mimic lipid composition (400 nm diameter, 0.5 mM lipids) in RB150 containing $MgCl_2$ (5 mM) and DTT (1 mM) at room temperature for 300 s. During incubation, turbidity changes in the Rab-liposome–mixed reactions were monitored by measuring the absorbance at 400 nm. The protein-to-lipid molar ratios used for these turbidity reactions were from 1:1000 to 1:125 as indicated.

the very high potency of these two endosomal Rabs to directly catalyze membrane-tethering reactions *in vitro*, consistent with our prior study on membrane tethering mediated by human Rabs (18). Moreover, by assaying high protein concentrations such as 4 μM Rab (protein-to-lipid ratio, 1:125), we found that not only Rab5a and Rab7a (Fig. 2, *C* and *D*) but also all of the other endosomal Rabs (Rab4a, Rab9a, Rab11a, and Rab14) retained the significant intrinsic capacity to initiate efficient tethering of synthetic liposomes by themselves (Fig. 2, *B*, *E*, *F*, and *G*). These data led us to propose the conserved function for all endosomal Rab-family GTPases to physically link two distinct lipid bilayers together for membrane-tethering events. It is also noteworthy that the observed Rab-mediated membrane-tethering reactions were driven by homotypic Rab-Rab pairing specifically but not by promiscuous Rab-Rab interactions (supplemental Fig. S2).

To what extent can the Rab protein densities on a membrane surface used in the current liposome turbidity assays (Fig. 2) recapitulate the physiological conditions at subcellular membranes in mammalian cells? Using synaptic vesicles as a model of a trafficking organelle, previous comprehensive proteomic and lipidomic analyses of highly purified synaptic vesicles from rat brain determined the average copy numbers per vesicle of the major protein constituents including Rab-family GTPases (29). Those quantitative data indicate that, on average, ~10 copies of Rab3a and 15 copies of the other Rab GTPases, thus 25 copies of Rab proteins in total, are present in each single purified synaptic vesicle (29). Assuming (i) this copy number of synaptic Rabs (25 copies/vesicle), (ii) a mean outer diameter of synaptic vesicles of 42 nm (29), (iii) a typical bilayer thickness of 4 nm (30), and (iv) an average area occupied by a single phospholipid molecule of 0.65 nm^2 (30), we estimated the surface areas of the outer and inner lipid layers of synaptic vesicles (5,540 nm^2 and 3,630 nm^2, respectively) that bore 14,100 lipid molecules in total, thereby giving an approximate Rab protein-to-lipid molar ratio of 1:560 (25 Rab/vesicle, 14,100 lipids/vesicle). It should be noted that, in the current chemically defined system, Rab5a and Rab7a (at least) can trigger rapid and efficient membrane tethering at a Rab-to-lipid molar ratio of 1:500 (Fig. 2, *C* and *D*), which is almost identical to the physiological ratio calculated above (Rab-to-lipid, 1:560). In addition to the Rab-to-lipid molar ratios, we also quantitatively estimated the membrane surface areas occupied by Rab proteins in the current reconstitution experiments (Fig. 2). Assuming that (i) Rab is typically a spherical 25-kDa protein with an average radius of 2.0 nm (31), (ii) all of the Rab-His_{12} molecules added to the reactions are stably attached to liposomal membranes containing a DOGS-NTA lipid (Fig. 2*A*), and (iii) a single 400-nm-diameter liposome contains 1,520,000 lipid molecules (total surface area, 985,000 nm^2, and surface area/lipid, 0.65 nm^2) (30), the percentage of membrane surface coverage by Rab proteins was calculated to be in the range of 3.79 to 30.3% (0.5–4.0 μM Rab proteins; Rab-to-lipid ratio, 1:1000–1:125) (Fig. 2). These estimated values of surface coverage by Rab proteins imply that Rab proteins occupy only a minor portion of the membrane surface area of liposomes used in the turbidity assays and thus appear to have plenty of space to interact and cooperate with other proteins and lipids on the membranes. Taken together, the Rab-to-lipid molar ratios and the membrane surface areas occupied by Rabs that we estimated above support the idea that endosomal Rab proteins can drive rapid and efficient membrane tethering *in vitro* under the physiological or physiologically relevant conditions that mimic subcellular membranes in mammalian cells.

Our data on the current liposome turbidity assays have revealed the conserved membrane-tethering potency of endosomal Rab proteins in the context of a physiologically relevant function (Fig. 2, *B–G*). Next, we asked whether the intrinsic membrane-tethering potency of human Rabs is a specialized function exclusively for Rab-family small GTPase proteins among the Ras-superfamily GTPases (24) and, moreover, for the Rab proteins that are specifically localized at the endosomal compartments. To address this question, we performed turbidity assays for the HRas protein as the model of a non-Rab Ras-superfamily GTPase (Fig. 3, *A* and *B*) and for two of the well-studied non-endosomal Rab proteins, Rab1a in ER-to-Golgi traffic and Rab3a in exocytosis (Fig. 3, *A*, *C*, and *D*), with the same range of protein concentrations as tested in Fig. 2, *B–G* (0.5–4.0 μM HRas or Rab proteins; protein-to-lipid molar ratios, 1:1000–1:125). Indeed, HRas had little membrane-tethering potency, with no significant increase in the turbidity of liposomes when assayed even at the highest HRas protein concentrations of 4.0 μM (HRas-to-lipid, 1:125) (Fig. 3*B*). Nevertheless, both of the non-endosomal Rab GTPases tested, Rab1a and Rab3a, retained the intrinsic capacity to directly induce efficient membrane tethering of synthetic liposomes (Fig. 3, *C* and *D*), as shown earlier with six endosomal Rabs (in Fig. 2). It should be noted that the difference of the *in vitro* membrane-tethering potency between different Rab-family members and also between Rab proteins and HRas does not simply rely on their attachment to liposomal membranes in the tethering reactions (Fig. 4). To examine the membrane association of Rab and HRas proteins in the current systems, liposome co-sedimentation assays were employed (Fig. 4*A*) using the same experimental conditions as in the liposome turbidity assays (Figs. 2 and 3, protein-to-lipid 1:500), which demonstrated that all of the tested Rab-family and HRas proteins comparably and stably bound to the liposomal membranes (Fig. 4, *B–J*). Thus, our data from the turbidity assays (Figs. 2 and 3) suggest that the intrinsic potency to physically tether two opposing membranes is selectively encoded in the Rab-family members among the Ras-superfamily GTPases and likely to be fully conserved through all the Rab-family members functioning in the endocytic and secretory pathways.

To further confirm the intrinsic membrane-tethering capacity of Rab-family GTPases as their genuine function, we employed fluorescence microscopic observations of the reconstituted reactions of Rab-mediated membrane tethering (Fig. 5). The tethering reactions were incubated with rhodamine (Rh)-labeled fluorescent liposomes (0.5 mM lipids, 1000-nm diameter) and Rab-family or HRas proteins (4 μM proteins; protein-to-lipid, 1:125) (Fig. 5*A*) as in the liposome turbidity assays (Figs. 2 and 3). Strikingly, whereas only small particles of non-tethered liposomes were observed when incubated in the absence of any Rab proteins (Fig. 5, *B* and *C*) or with the control HRas protein (Fig. 5, *T* and *U*), all of the tested

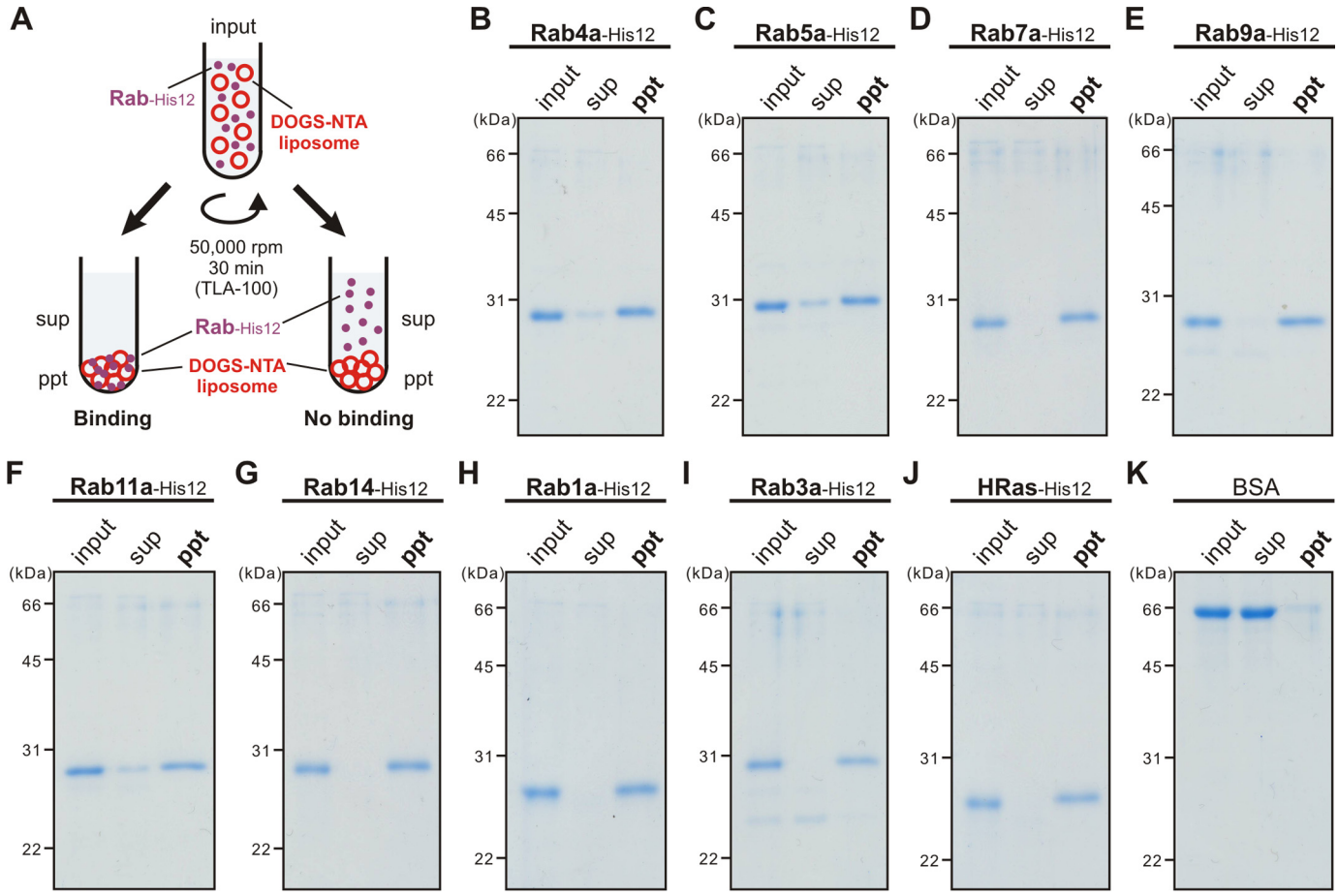

Figure 4. Membrane association of Rab-His$_{12}$ proteins onto DOGS-NTA–bearing liposomes. *A*, schematic representation of liposome co-sedimentation assays for testing membrane attachment of the Rab-His$_{12}$ proteins used in Figs. 2 and 3. *B–K*, Rh-labeled liposomes (400 nm diameter, 1 mM total lipids in final) were incubated (30 °C, 30 min) with Rab4a-His$_{12}$ (*B*), Rab5a-His$_{12}$ (*C*), Rab7a-His$_{12}$ (*D*), Rab9a-His$_{12}$ (*E*), Rab11a-His$_{12}$ (*F*), Rab14-His$_{12}$ (*G*), Rab1a-His$_{12}$ (*H*), Rab3a-His$_{12}$ (*I*), HRas-His$_{12}$ (*J*), and BSA for a negative control (*K*) (2 μM final for each) and ultracentrifuged (50,000 rpm, 30 min, 4 °C). The supernatants (*sup*) and precipitates (*ppt*) obtained were analyzed by SDS-PAGE and Coomassie Blue staining.

endosomal and non-endosomal Rab proteins (Rab4a, Rab5a, Rab7a, Rab9a, Rab11a, Rab14, Rab1a, and Rab3a) were able to specifically induce the formation of substantial massive clusters of liposomes (Fig. 5, *D–S*). Liposome clusters observed in the fluorescence images were then quantitatively analyzed for particle size distributions (Fig. 6*A*), yielding average sizes of Rab-mediated liposome clusters ranging from 7.8 to 55 μm^2, which are much larger than those of the control reactions (0.92 and 0.80 μm^2 for the reactions without any Rabs and with HRas, respectively) (Fig. 6*B*). Therefore, our morphological analyses of Rab-mediated membrane-tethering reactions by fluorescence microscopy were fully consistent with the results obtained in the liposome turbidity assays (Figs. 2 and 3), thus further establishing the working model that Rab-family proteins themselves act as a *bona fide* membrane tether to directly and physically link two distinct lipid bilayers of subcellular membranes in intracellular membrane tethering.

Class V myosins, the Rab11a effectors, strongly and selectively promote membrane tethering mediated by the cognate Rab GTPase

By comprehensively and quantitatively characterizing *in vitro* membrane-tethering reactions reconstituted with the chemically defined lipid bilayers and purified recombinant proteins of eight Rab GTPases in human (Rab1a, Rab3a, Rab4a, Rab5a, Rab7a, Rab9a, Rab11a, and Rab14) (Figs. 1–6), we now have established that Rab-family proteins genuinely have the intrinsic potency to directly and specifically tether two distinct lipid bilayers together in the context of a physiologically relevant function. Nevertheless, it is noteworthy that there appears to be wide variability in the tethering capacity of human Rab-family GTPases, although Rab proteins share the highly conserved amino acid sequences and tertiary structures of their Ras-superfamily GTPase domains (Fig. 1*A*) (24, 32), which exhibited comparable GTP hydrolysis activities for all eight Rabs tested (Fig. 1*C*). As typical instances of the variability in Rab-mediated tethering potency, Rab5a and Rab7a could trigger rapid membrane tethering at protein-to-lipid molar ratios of 1:500 (Fig. 2, *C* and *D*), whereas most of the other Rabs (Rab1a, Rab4a, Rab9a, Rab11a, and Rab14) showed little or no tethering activity under the same conditions of Rab density on the membrane surface (Rab-to-lipid, 1:500) (Fig. 2, *B* and *E–G*, and Fig. 3*C*). These results led us to hypothesize that (i) the intrinsic tethering activity of Rab proteins is negatively autoregulated in general, especially in the case of the Rabs that cause very slow and inefficient membrane tethering by themselves (Rab1a, Rab4a, Rab9a, Rab11a, and Rab14); and thus (ii) specific

Rab-interacting proteins (Rab effectors) drastically enhance the capacity of their cognate Rabs to drive membrane tethering. To test this hypothesis, we next attempted to reconstitute membrane-tethering reactions with Rab11a, which had exhibited the lowest tethering potency among the eight Rab proteins tested in the earlier liposome turbidity assays (Fig. 2*F*), and the

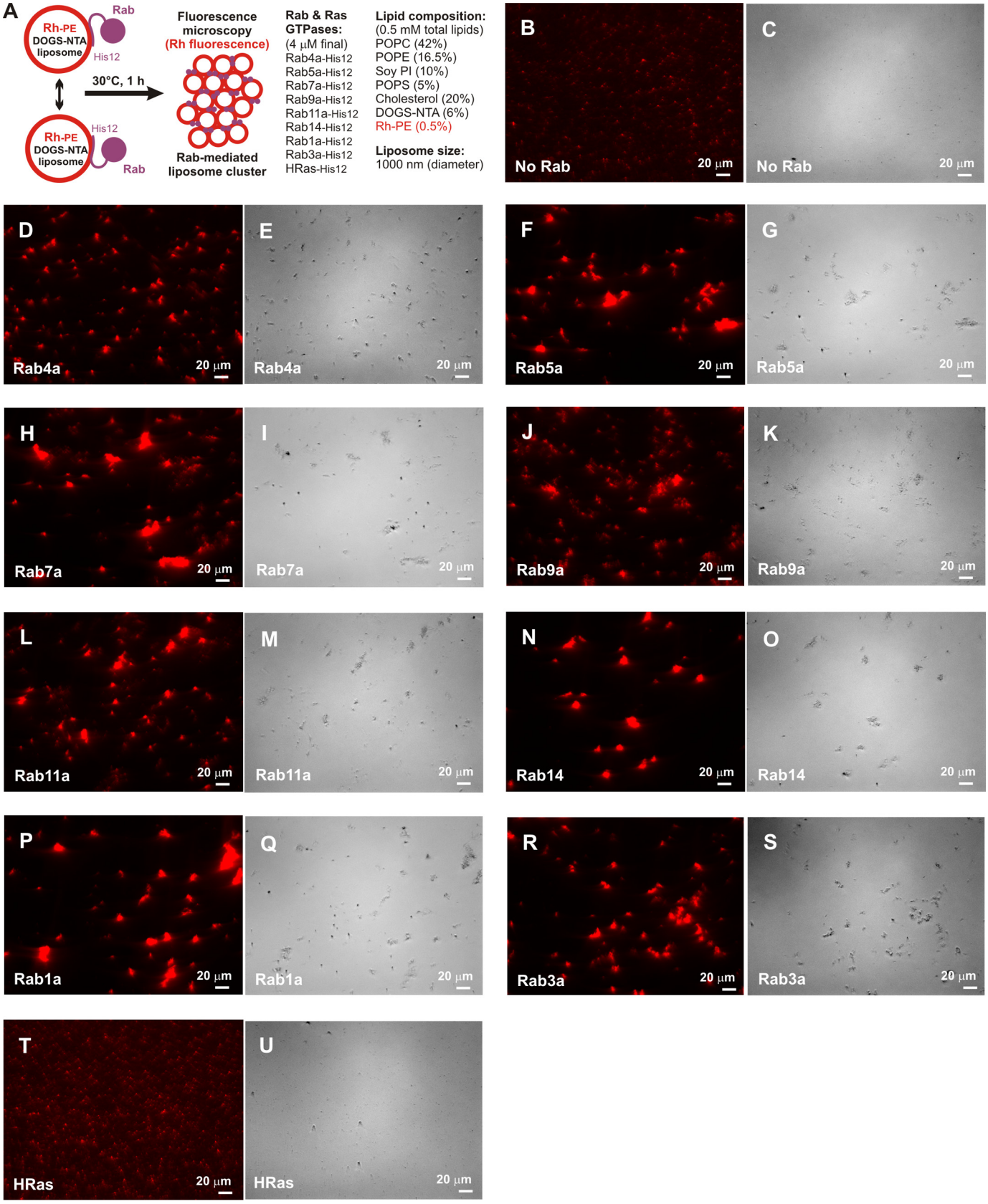

A

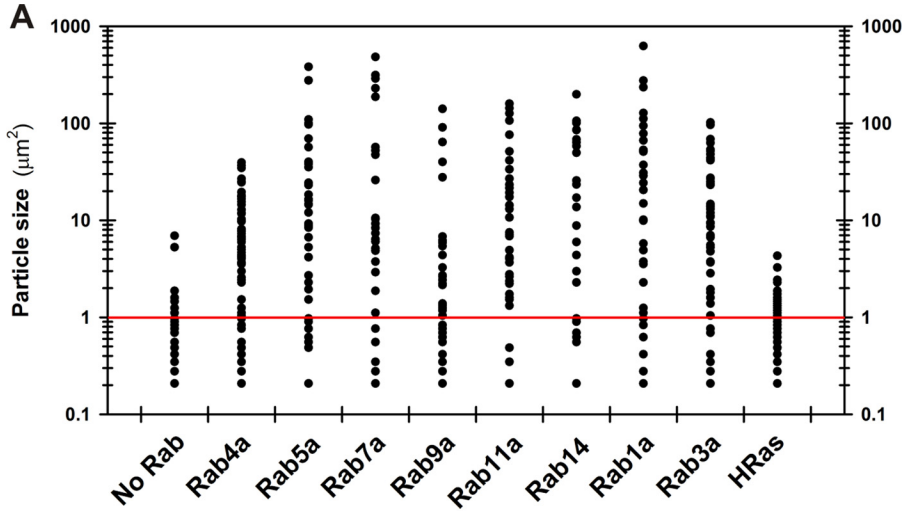

B

Rab protein	Particle number	Average size (μm^2)
No Rab	38	0.92
Rab4a-His12	67	7.8
Rab5a-His12	45	32
Rab7a-His12	33	53
Rab9a-His12	55	7.9
Rab11a-His12	35	27
Rab14-His12	25	37
Rab1a-His12	36	55
Rab3a-His12	51	18
HRas-His12	96	0.80

Figure 6. Particle size distributions of liposome clusters induced by Rab-mediated membrane tethering. *A*, particle sizes of the Rab-mediated liposome clusters observed in the fluorescence images shown in Fig. 5. *B*, particle numbers and average sizes (μm^2) of the Rab-mediated liposome clusters observed in the fluorescence images shown in Fig. 5.

cognate Rab11a effectors, class V myosin motor proteins (Myo5A and Myo5B) (Fig. 7). Although none of the Rab11a effectors identified, except for the Exoc6/Sec15 exocyst subunit (33–35), has ever been proposed or reported to be directly involved in membrane-tethering events (4, 5, 7), it has been thought that, as Rab effectors, class V myosins directly bind and cooperate with the cognate Rab11a on transport vesicles to regulate the specificity of membrane trafficking (36–39).

To reconstitute the Rab11a- and class V myosin–dependent membrane-tethering reaction in a chemically defined system, we purified the globular tail domains of class V myosin proteins (Myo5A-GTD and Myo5B-GTD) in humans, which correspond to C-terminal residues 1534–1855 of myosin 5a (Myo5A) and residues 1526–1848 of myosin 5b (Myo5B) (Fig. 7, *A* and *B*). It should be noted that previous biochemical and structural studies indicate that these globular tail domains of

Figure 5. Rab-mediated membrane tethering induces the formation of massive liposome clusters. *A*, schematic representation of fluorescence microscopic observations of Rab-mediated liposome clusters. *B–U*, fluorescence images (*B*, *D*, *F*, *H*, *J*, *L*, *N*, *P*, *R*, and *T*) and bright-field images (*C*, *E*, *G*, *I*, *K*, *M*, *O*, *Q*, *S*, and *U*) of Rab-mediated liposome clusters. Fluorescently labeled liposomes bearing Rh-PE (1000 nm diameter, 0.5 mM lipids in final) were incubated at 30 °C for 1 h in the absence (*B* and *C*) and presence of the Rab- and Ras-family GTPases (4 μM each in final), including Rab4a-His_{12} (*D* and *E*), Rab5a-His_{12} (*F* and *G*), Rab7a-His_{12} (*H* and *I*), Rab9a-His_{12} (*J* and *K*), Rab11a-His_{12} (*L* and *M*), Rab14-His_{12} (*N* and *O*), Rab1a-His_{12} (*P* and *Q*), Rab3a-His_{12} (*R* and *S*), and HRas-His_{12} (*T* and *U*), and subjected to fluorescence microscopy. *Scale bars*: 20 μm.

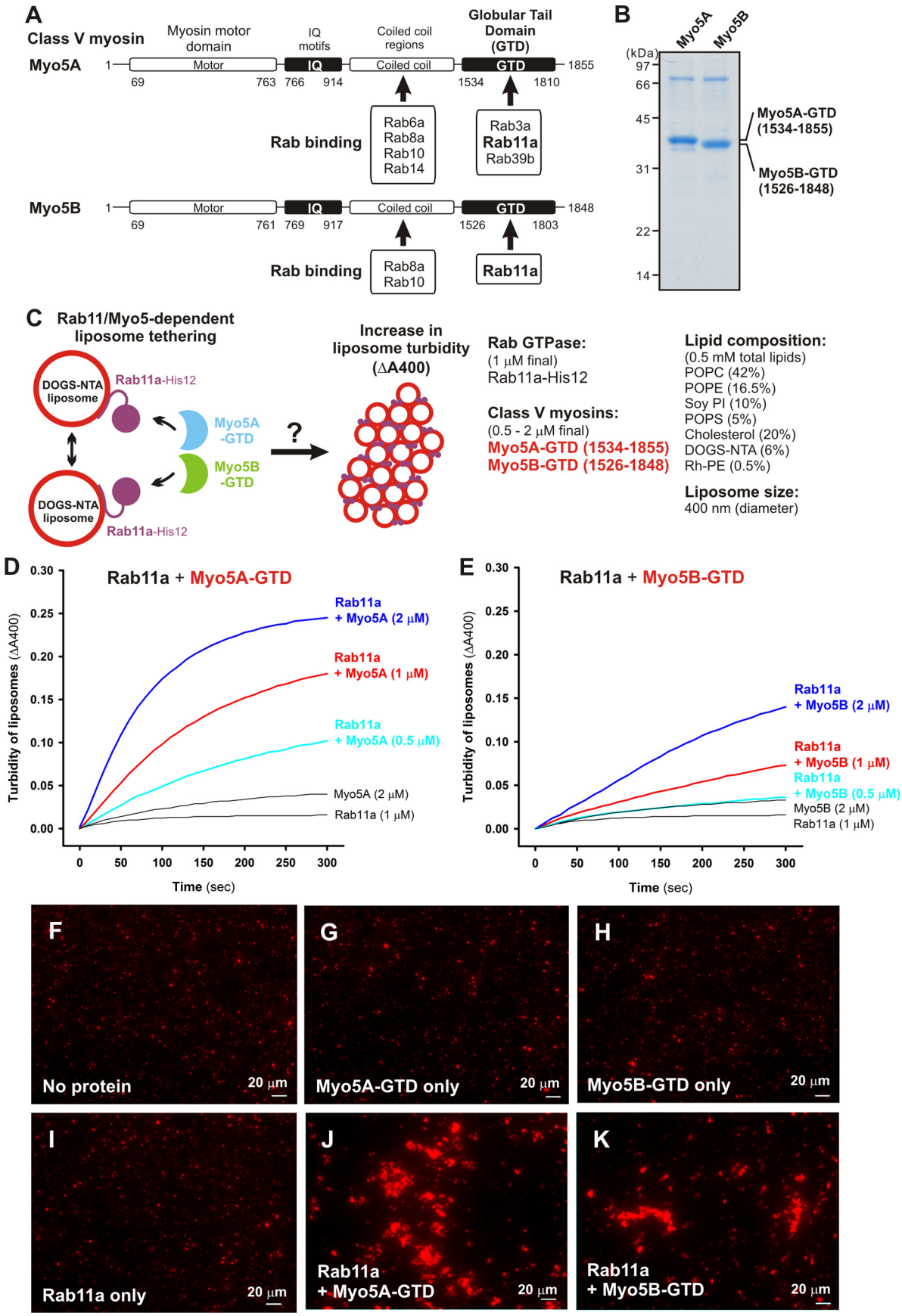
A
Class V myosin
Myosin motor domain
IQ motifs
Coiled coil regions
Globular Tail Domain (GTD)
Myo5A
Motor
IQ
Coiled coil
GTD
1
69
763
766
914
1534
1810
1855
Rab binding
Rab6a
Rab8a
Rab10
Rab14
Rab3a
Rab11a
Rab39b
Myo5B
Motor
IQ
Coiled coil
GTD
1
69
761
769
917
1526
1803
1848
Rab binding
Rab8a
Rab10
Rab11a
B
Myo5A
Myo5B
(kDa)
97
66
45
31
22
14
Myo5A-GTD (1534-1855)
Myo5B-GTD (1526-1848)
C
Rab11/Myo5-dependent liposome tethering
DOGS-NTA liposome
Rab11a-His12
Myo5A -GTD
Myo5B -GTD
DOGS-NTA liposome
Rab11a-His12
?
Increase in liposome turbidity (ΔA400)
Rab GTPase:
(1 μM final)
Rab11a-His12
Class V myosins:
(0.5 - 2 μM final)
Myo5A-GTD (1534-1855)
Myo5B-GTD (1526-1848)
Lipid composition:
(0.5 mM total lipids)
POPC (42%)
POPE (16.5%)
Soy PI (10%)
POPS (5%)
Cholesterol (20%)
DOGS-NTA (6%)
Rh-PE (0.5%)
Liposome size:
400 nm (diameter)
D
Rab11a + Myo5A-GTD
Turbidity of liposomes (ΔA400)
Time (sec)
Rab11a + Myo5A (2 μM)
Rab11a + Myo5A (1 μM)
Rab11a + Myo5A (0.5 μM)
Myo5A (2 μM)
Rab11a (1 μM)
E
Rab11a + Myo5B-GTD
Turbidity of liposomes (ΔA400)
Time (sec)
Rab11a + Myo5B (2 μM)
Rab11a + Myo5B (1 μM)
Rab11a + Myo5B (0.5 μM)
Myo5B (2 μM)
Rab11a (1 μM)
F
No protein
20 μm
G
Myo5A-GTD only
20 μm
H
Myo5B-GTD only
20 μm
I
Rab11a only
20 μm
J
Rab11a + Myo5A-GTD
20 μm
K
Rab11a + Myo5B-GTD
20 μm

Myo5A and Myo5B are necessary and sufficient for binding to Rab11a (Fig. 7*A*) (39–42). Using purified Myo5A-GTD and Myo5B-GTD proteins (Fig. 7*B*), we employed liposome turbidity assays to test whether class V myosin proteins have an effect on membrane-tethering reactions mediated by the cognate Rab11a (Fig. 7, *C–E*). Strikingly, Rab11a-mediated tethering was strongly promoted by the addition of an equimolar amount (1 μM) or a 2-fold molar excess (2 μM) of Myo5A-GTD (Fig. 7*D*) or Myo5B-GTD (Fig. 7*E*) over Rab11a (1 μM; Rab-to-lipid ratio, 1:500), thus exhibiting much higher initial rates of increased turbidity than those in the absence of Myo5-GTD proteins. We also showed that a non-interacting control protein (BSA) had no stimulatory effect on the tethering activity of Rab11a (supplemental Fig. S3). It should be noted that the molar ratio of the yeast ortholog of class V myosins (Myo2p) to its cognate Rab protein (Sec4p) in yeast cells was estimated to be about an equimolar ratio using quantitative immunoblots (43), indicating that the Myo5-to-Rab molar ratios used in the current reconstitution assays (Fig. 7, *C–E*) are not far from those found under physiological conditions. The morphological changes in the liposomes in the tethering reactions with Rab11a and Myo5-GTD proteins were also analyzed by fluorescence microscopy (Fig. 7, *F–K*), which indicated that Rab11a and Myo5-GTD proteins synergistically and specifically induced the formation of massive clusters of liposomes (Fig. 7, *J* and *K*). Thus, the current results from these two independent assays in a chemically defined system uncover the novel function of class V myosins as directly supporting membrane tethering mediated by their cognate Rab11a GTPase.

Because class V myosins are recognized as Rab effectors that, in general, selectively interact with the GTP-bound form of Rab proteins (38), we next tested the guanine nucleotide dependence of Rab11a- and Myo5-GTD–mediated membrane tethering by employing liposome turbidity assays (Fig. 8*A*). Indeed, the addition of GTP (1 mM) drastically stimulated the synergistic action of Rab11a and Myo5A-GTD (Fig. 8*B*) or Myo5B-GTD (Fig. 8*C*) in driving rapid membrane tethering, but the presence of GTP had no effect on the tethering reactions of either Rab11a or Myo5-GTD proteins alone (Fig. 8, *B* and *C*). The GTP independence of membrane tethering mediated by Rab11a alone is consistent with our previous data on Rab5a and other Rab isoforms (18). Considering that the targeting of Rab proteins to subcellular membrane compartments is mediated by GDP/GTP exchange and Rab-guanine nucleotide exchange factors (44–46), these results suggest that the stable attachment of Rab-His_{12} proteins on DOGS-NTA–bearing membranes in the current system can bypass the GTP requirement for Rab-only tethering reactions (Fig. 8, *B* and *C*) (18). Direct stimulation by GTP on Rab11a/Myo5-GTD–dependent membrane tethering was shown to have a very specific effect when added to the variable GTP concentrations ranging from 1 μM to 1 mM (Fig. 8, *D* and *E*) and assayed with the other guanine nucleotides, GDP and GTPγS (Fig. 8, *F* and *G*). Our data therefore reflect that Myo5-GTD proteins greatly enhance the tethering activity of Rab11a in a GTP-dependent manner, suggesting that the protein-protein interactions of Myo5-GTD proteins with membrane-bound Rab11a-GTP proteins are required to facilitate membrane tethering. To experimentally test the association of Myo5-GTD proteins with Rab11a proteins on liposomal membranes, liposome co-sedimentation assays were performed under the typical conditions used for the turbidity assays shown in Fig. 8 (Rab-to-lipid ratio, 1:500; Rab-to-Myo5-GTD ratio, 1:1; 1 mM GTP) (Fig. 9*A*). However, we found that the amounts of Myo5A-GTD (Fig. 9*B*) and Myo5B-GTD (Fig. 9*E*) bound to and co-isolated with Rab11a-attached liposomes were comparable with those of the control reactions with protein-free liposomes in the absence of Rab11a-His_{12} (Fig. 9, *C* and *F*) or in the presence of untagged Rab11a lacking a His_{12} tag (Fig. 9, *D* and *G*). This indicates, unexpectedly, that the membrane association of Myo5-GTD proteins was not significantly promoted by the recruitment of Rab11a on a liposomal membrane surface. Considering that rapid and efficient Rab11a-mediated membrane tethering definitely relied on the presence of Myo5-GTD proteins and GTP in the current reconstitution system (Figs. 7 and 8), our results from the co-sedimentation assays (Fig. 9) may imply that a specific, but not stable, interaction is required for the tethering reaction. Myo5-GTD in this assay appears to act as a "catalyst" of conformational change in Rab11a that is required for increased Rab-Rab interactions, and this conformational change may be additionally facilitated by GTP binding.

Our current studies have uncovered the novel function of class V myosins in directly promoting membrane tethering mediated by their cognate Rab11a GTPase in a GTP-dependent manner, by thoroughly characterizing reconstituted membrane tethering in chemically defined systems with purified Rab11a and Myo5-GTD proteins (Figs. 7–9). However, it could still be argued that Myo5-GTD proteins can non-physiologically induce tethering or aggregation of liposomal membranes coated by other non-cognate Rab-His_{12} proteins or even coated by any types of soluble protein modified with a polyhistidine tag. In this context, to more strictly validate and further explore the specificity of Rab11a/Myo5-GTD–dependent membrane tethering, we used liposome turbidity assays in the presence of Myo5-GTD proteins (Fig. 10*A*), not only for the cognate Rab11a but also for the other four Rab proteins (Rab1a, Rab4a, Rab9a, and Rab14), which had shown relatively slow and inefficient membrane tethering by themselves, similar to Rab11a

Figure 7. Class V myosin globular tail domains, Myo5A-GTD and Myo5B-GTD, strongly stimulate Rab11a-dependent membrane tethering. *A*, schematic representation of class V myosins in humans, Myo5A and Myo5B, showing their amino acid residues and domains including myosin motor domains, IQ motifs, coiled-coil regions, and GTDs. Representative Myo5-interacting Rab GTPases and the Rab-binding regions in Myo5A and Myo5B are indicated. *B*, the Coomassie Blue-stained gel of purified Myo5A-GTD and Myo5B-GTD proteins, which are comprised of amino acid residues 1534–1855 and 1526–1848, respectively. *C*, schematic representation of liposome turbidity assays for testing Rab11a- and Myo5-GTD–dependent liposome tethering (shown in *D* and *E*). *D* and *E*, liposome turbidity assays were employed with Rab11a-His_{12} (1 μM final) as described in the legend for Fig. 2*F* but in the presence of Myo5A-GTD (*D*) and Myo5B-GTD (*E*) (0.5–2 μM final). *F–K*, fluorescence images of Rab11a-mediated liposome clusters in the presence of Myo5-GTDs. Rab11a-His_{12} (3 μM final) and Myo5A-GTD or Myo5B-GTD (3 μM final) were preincubated at 30 °C for 30 min, mixed with Rh-labeled liposomes (1000 nm diameter, 0.8 mM lipids in final), incubated further (30 °C, 30 min), and subjected to fluorescence microscopy (*J* and *K*). For a control, Rab11a-His_{12}, Myo5-GTD, or both were omitted from the reactions where indicated (*F–I*). *Scale bars*: 20 μm.

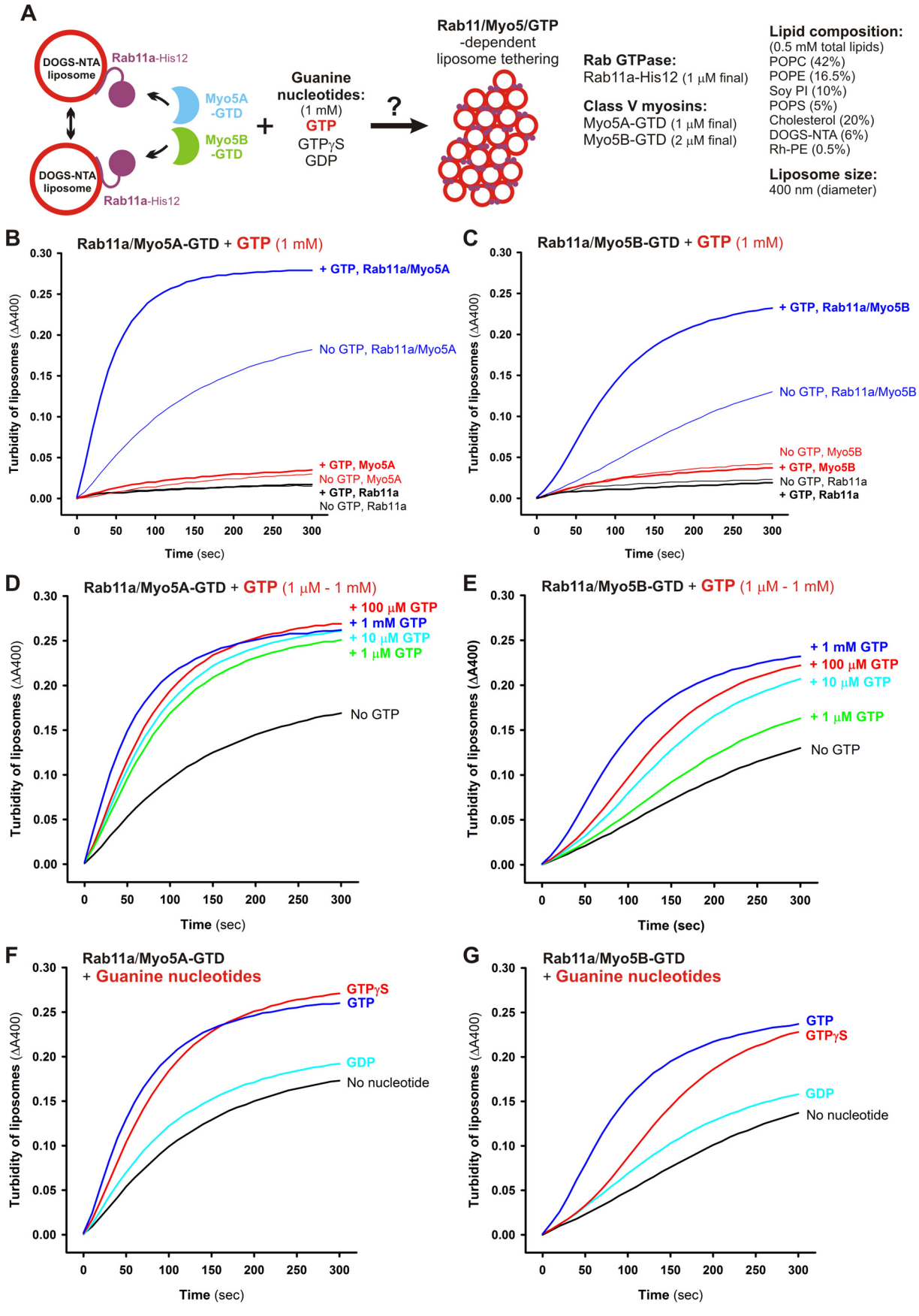
A
DOGS-NTA liposome
Rab11a-His12
Myo5A -GTD
Myo5B -GTD
DOGS-NTA liposome
Rab11a-His12
Guanine nucleotides:
(1 mM)
GTP
GTPγS
GDP
?
Rab11/Myo5/GTP -dependent liposome tethering
Rab GTPase:
Rab11a-His12 (1 μM final)
Class V myosins:
Myo5A-GTD (1 μM final)
Myo5B-GTD (2 μM final)
Lipid composition:
(0.5 mM total lipids)
POPC (42%)
POPE (16.5%)
Soy PI (10%)
POPS (5%)
Cholesterol (20%)
DOGS-NTA (6%)
Rh-PE (0.5%)
Liposome size:
400 nm (diameter)
B
Rab11a/Myo5A-GTD + GTP (1 mM)
+ GTP, Rab11a/Myo5A
No GTP, Rab11a/Myo5A
+ GTP, Myo5A
No GTP, Myo5A
+ GTP, Rab11a
No GTP, Rab11a
Turbidity of liposomes (ΔA400)
Time (sec)
C
Rab11a/Myo5B-GTD + GTP (1 mM)
+ GTP, Rab11a/Myo5B
No GTP, Rab11a/Myo5B
No GTP, Myo5B
+ GTP, Myo5B
No GTP, Rab11a
+ GTP, Rab11a
Turbidity of liposomes (ΔA400)
Time (sec)
D
Rab11a/Myo5A-GTD + GTP (1 μM - 1 mM)
+ 100 μM GTP
+ 1 mM GTP
+ 10 μM GTP
+ 1 μM GTP
No GTP
Turbidity of liposomes (ΔA400)
Time (sec)
E
Rab11a/Myo5B-GTD + GTP (1 μM - 1 mM)
+ 1 mM GTP
+ 100 μM GTP
+ 10 μM GTP
+ 1 μM GTP
No GTP
Turbidity of liposomes (ΔA400)
Time (sec)
F
Rab11a/Myo5A-GTD
+ Guanine nucleotides
GTPγS
GTP
GDP
No nucleotide
Turbidity of liposomes (ΔA400)
Time (sec)
G
Rab11a/Myo5B-GTD
+ Guanine nucleotides
GTP
GTPγS
GDP
No nucleotide
Turbidity of liposomes (ΔA400)
Time (sec)

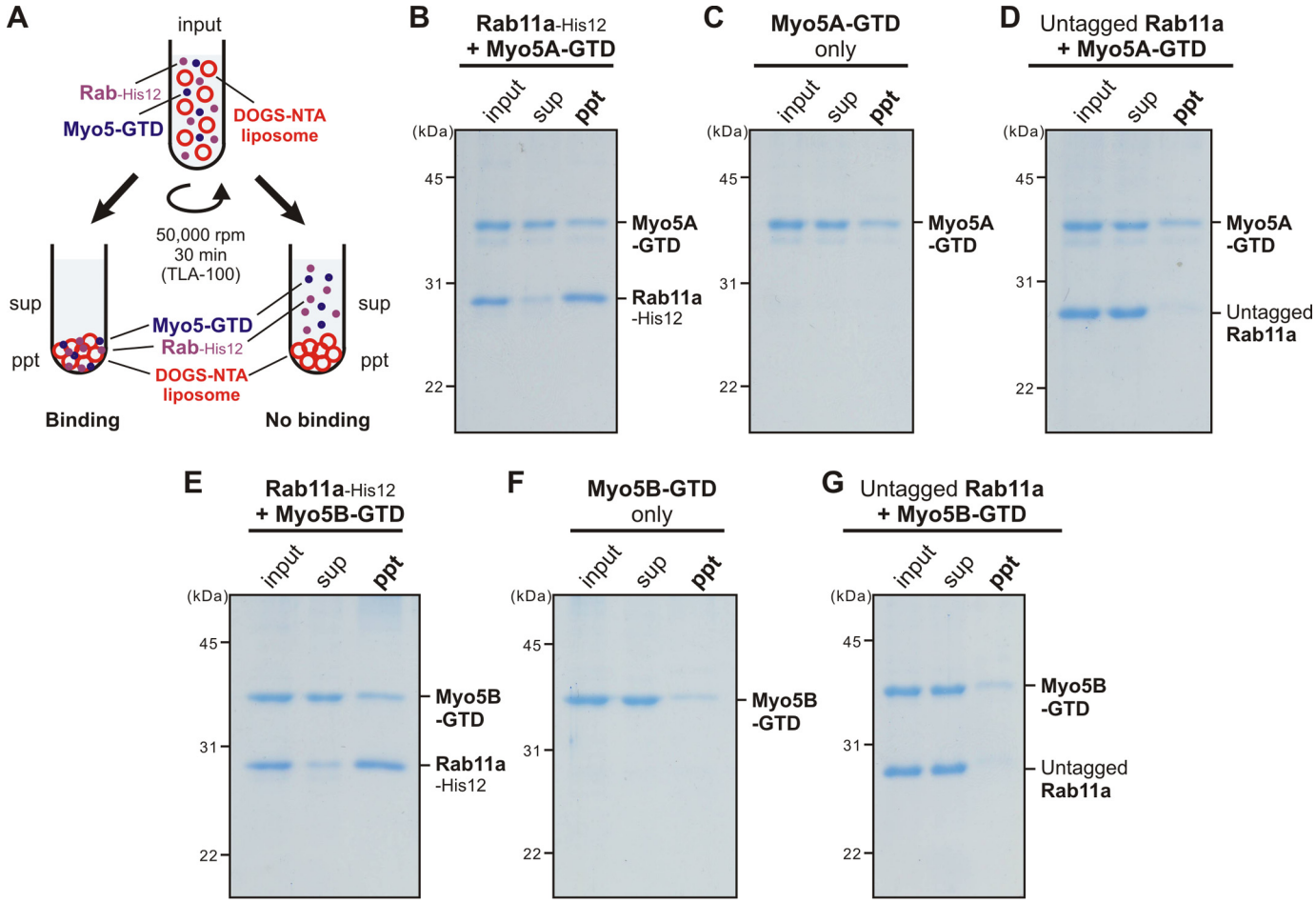

Figure 9. Membrane association of Myo5-GTD proteins with Rab11a-anchored liposomes. *A*, schematic representation of liposome co-sedimentation assays for testing membrane binding of Myo5A-GTD and Myo5B-GTD to Rab11a-bound liposomes. *B–G*, liposome co-sedimentation assays were employed as described in the legend for Fig. 4, with Rh-labeled liposomes (400 nm diameter, 1 mM lipids) and Rab11a-His_{12} (2 μM) (*B* and *E*) but in the presence of Myo5A-GTD (2 μM) (*B–D*), Myo5B-GTD (2 μM) (*E–G*), and GTP (1 mM). For a control, the reactions without Rab11a-His_{12} (*C* and *F*) or with the untagged form of Rab11a lacking a His_{12} tag (untagged Rab11a) (*D* and *G*) were also tested. The supernatants (*sup*) and precipitates (*ppt*) obtained were analyzed by SDS-PAGE and Coomassie Blue staining.

(Figs. 2 and 3). Although Rab11a and either Myo5A-GTD or Myo5B-GTD proteins synergistically triggered very rapid and efficient membrane tethering (Fig. 10, *B* and *C*), fully consistent with the results shown in Fig. 8, these Myo5-GTD proteins had only a minor or little effect on the tethering potency of Rab1a, Rab4a, Rab9a, and Rab14 (Fig. 10, *B* and *C*).

In addition to testing for Rab selectivity (Fig. 10), to further establish the specificity of Rab11a- and Myo5-dependent membrane tethering, we next tested whether the membrane attachment of Rab11a on both of two opposing membranes was critical to catalyzing the tethering reactions, by employing streptavidin bead–based liposome-tethering assays (18, 52) (Fig. 11, *A–C*) and fluorescence microscopy (Fig. 11, *D–G*). In the streptavidin bead–based assays, purified proteins of Rab11a-His_{12} and Myo5-GTDs were incubated with two types of the DOGS-NTA liposomes bearing either biotin-PE/Rh-PE or FL-PE (fluorescein-PE) and a streptavidin-coated bead (Fig. 11*A*). Following the incubation of the reaction mixtures, the FL fluorescence of the FL-PE liposomes co-isolated with the biotin-PE liposomes bound to the beads was measured to quantitatively evaluate the membrane-tethering capacities of these protein components (Fig. 11, *B* and *C*). Consistent with the results of the liposome turbidity assays and fluorescence microscopic observations depicted in Fig. 7, efficient membrane tethering was specifically triggered when both Rab11a and Myo5-GTD proteins were added to the reactions (Fig. 11*B*, *lanes 5* and *6*). However, strikingly, the tethering potency of Rab11a and Myo5-GTD was thoroughly abolished by omitting a DOGS-NTA lipid from one of the liposomes used, FL-PE liposomes (Fig. 11*C*, *lanes 2* and *4*). This finding implies that Rab11a needs

Figure 8. Guanine nucleotide dependence of Rab11a-mediated membrane tethering in the presence of Myo5A-GTD and Myo5B-GTD. *A*, schematic representation of liposome turbidity assays for testing Rab11a- and Myo5-GTD–dependent liposome tethering in the presence of GTP (shown in *B–G*). *B* and *C*, Rab11a/Myo5-dependent membrane tethering is strongly and specifically promoted by the addition of GTP. Liposome turbidity assays with Rab11a-His_{12} (1 μM) and Myo5A-GTD (1 μM) (*B*) or Myo5B-GTD (2 μM) (*C*) were performed as described in the legend for Fig. 7, *D* and *E*, but in the presence of GTP (1 mM). *D* and *E*, liposome turbidity assays were employed with Rab11a-His_{12} and Myo5A-GTD (*D*) or Myo5B-GTD (*E*), as described in *B* and *C*, in the presence of various concentrations of GTP (1 μM–1 mM). *F* and *G*, liposome turbidity assays were employed with Rab11a-His_{12} and Myo5A-GTD (*F*) or Myo5B-GTD (*G*), as described in *B* and *C*, in the presence of GTP, GTPγS, and GDP (each at 1 mM).

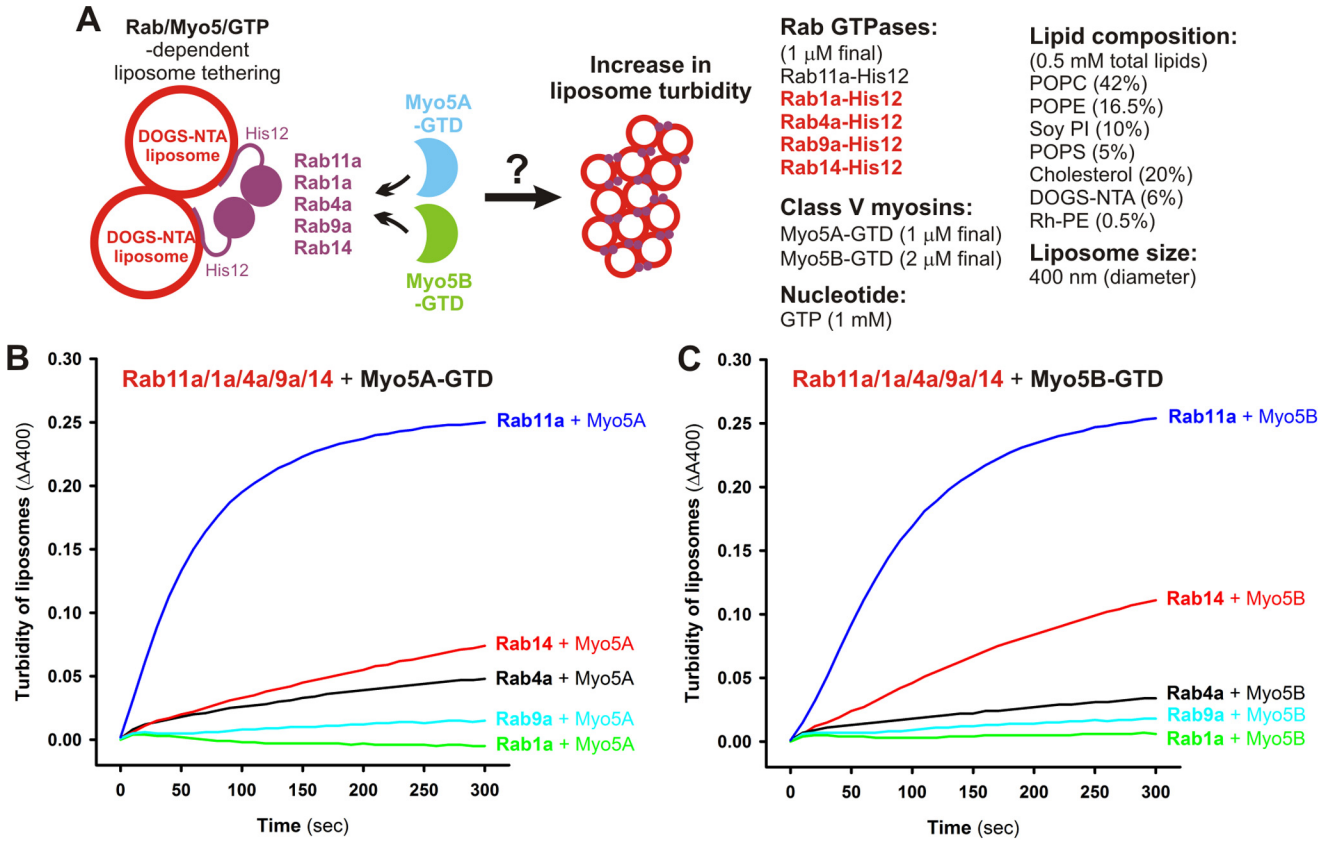

Figure 10. Myo5A-GTD and Myo5B-GTD selectively activate Rab11a-dependent membrane tethering. *A*, schematic representation of liposome turbidity assays (shown in *B* and *C*) for the various Rab GTPases (Rab11a, Rab1a, Rab4a, Rab9a, and Rab14) in the presence of Myo5-GTDs and GTP. *B* and *C*, Myo5-GTDs specifically promote efficient membrane tethering mediated by the cognate Rab GTPase, Rab11a. Liposome turbidity assays were employed using Myo5A-GTD (*B*) or Myo5B-GTD (*C*) and GTP, as described in the legend for Fig. 8, *B* and *C*, for Rab11a, Rab1a, Rab4a, Rab9a, and Rab14 GTPases.

to be anchored on both of two opposing membrane surfaces to initiate membrane tethering in the presence of Myo5-GTD. We then addressed the same issue, the requirement of membrane-bound Rab11a for tethering, by fluorescence microscopy using Rh- and FL-labeled liposomes (Fig. 11, *D*–*G*). As expected from the results of the bead-based tethering assays (Fig. 11, *B* and *C*), the addition of Rab11a and Myo5-GTD to the liposome suspensions induced the formation of massive liposome clusters bearing both the Rh-PE liposomes and the FL-PE liposomes (Fig. 11, *D* and *F*). Nevertheless, when tested with the Rh-PE liposomes lacking a DOGS-NTA lipid instead, Rab11a and Myo5-GTDs no longer had the capacity to support the stable association of the Rh-PE liposomes with the FL-PE liposome clusters (Fig. 11, *E* and *G*). Therefore, these results from two independent reconstitution assays clearly demonstrate that Rab11a- and Myo5-mediated membrane tethering requires the membrane attachment of Rab11a proteins on both of two opposing membranes destined to tether, thus establishing the need for the assembly of membrane-anchored Rab11a proteins in *trans* to physically link two distinct lipid bilayers in this tethering process.

Taken together, our data faithfully reflect that both Myo5A-GTD and Myo5B-GTD recognize and act exclusively upon the membrane-anchored form of the cognate Rab11a at the membrane surface of lipid bilayers, thereby selectively activating Rab11a-mediated membrane-tethering reactions driven by *trans*-Rab protein assemblies. These current findings from reconstituted membrane tethering with purified Rab and Myo5-GTD proteins (Figs. 7–11) provide new insights into how Rab GTPases on subcellular membranes (transport vesicles, organelle membranes, or the plasma membrane) and class V myosin motors on actin cytoskeletal tracks co-operate with each other to promote membrane tethering and how their functions synergistically contribute to the spatiotemporal specificity of membrane tethering and beyond.

Conclusions

Membrane tethering is one of the most critical and important processes for determining the specificity of membrane traffic in eukaryotic endomembrane systems, thus delivering the correct sets of cargoes (proteins, lipids, etc.) to the correct locations (organelles, the plasma membrane, the extracellular space, etc.) (8). Based on a large body of prior studies using genetic, cell biological, biochemical, and structural biological approaches on this essential membrane-tethering process, we generally recognize that a number of diverse but specific types of "Rab effectors" have been described as so-called tethering factors, such as coiled-coil tethering proteins and multisubunit tethering complexes (10, 47, 48). However, for the most part, it remains ambiguous indeed whether these "tethering factors" identified constitute a *bona fide* membrane tether that physically links two distinct opposing membranes by itself and, furthermore, whether they are even involved directly in membrane-tethering events (17). In this context, to thoroughly define and characterize the molecular functions in membrane

tethering for Rab-family GTPases and class V myosin cytoskeletal motor proteins as specific Rab effectors, we undertook to recapitulate the membrane-tethering machinery in chemically defined systems reconstituted with synthetic lipid bilayers of liposomes and purified proteins of human Rab GTPases and class V myosins (Figs. 1, 2, and 7).

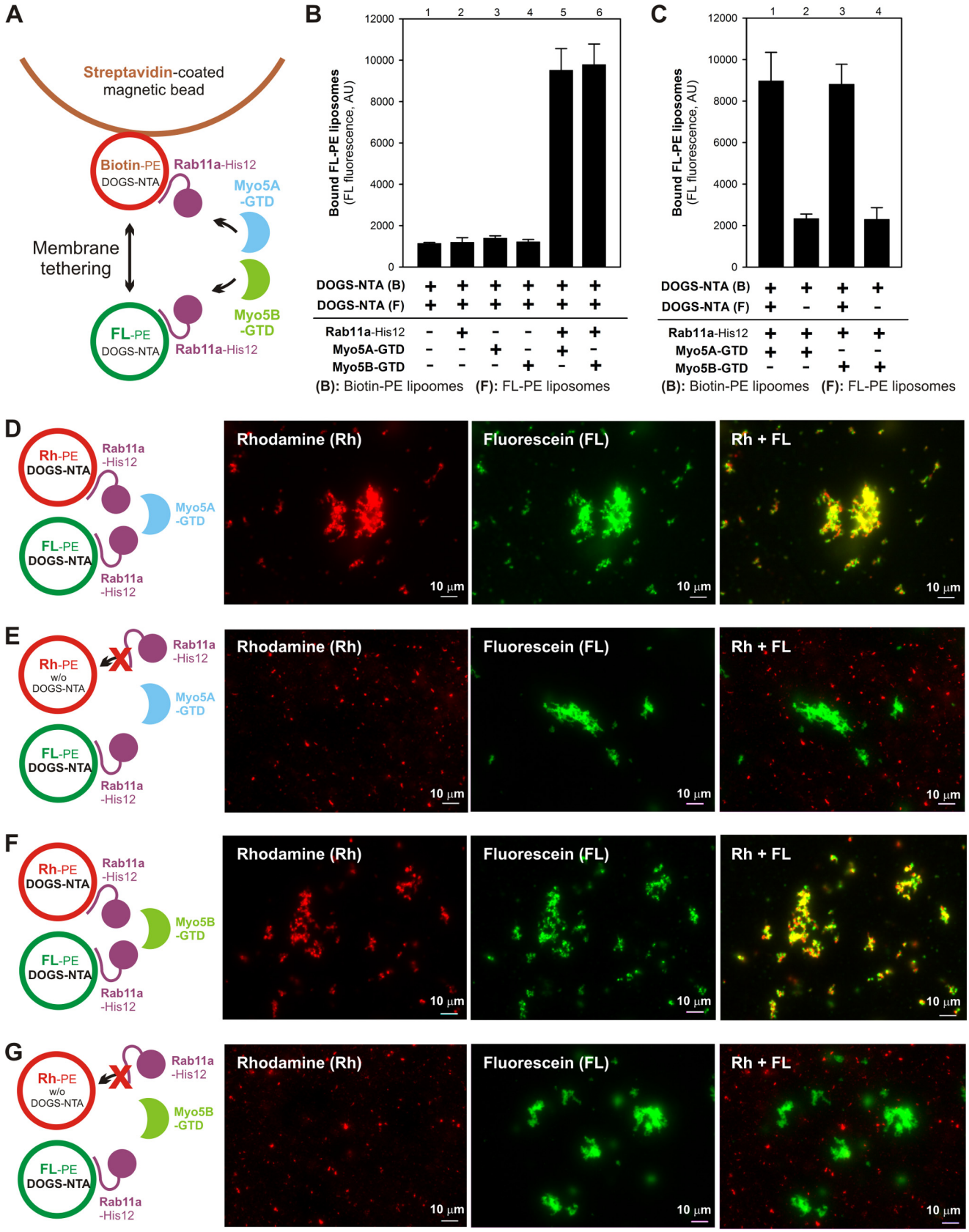

Our current *in vitro* reconstitution studies present three new findings that support the working model of intracellular membrane tethering mediated by Rab-family GTPases as a genuine membrane tether. (i) All eight Rab proteins tested, including both endosomal and non-endosomal Rabs, have the intrinsic capacity to physically tether two opposing membranes under experimental conditions that mimic the lipid composition and Rab density of subcellular organelles/vesicles in mammalian cells, establishing the conserved tethering function of the Rab-family members (Figs. 2, 3, and 5). (ii) The tethering capacity of Rab proteins is a specific function among the Ras-superfamily GTPases and yet highly variable for each of different Rab proteins (Figs. 2, 3, and 5), which suggests that the Rab subfamily–specific motifs could be the regions responsible for controlling the membrane-tethering potency of each Rab (49, 50). (iii) Finally, the Rab effectors, class V myosins, can drastically and specifically promote membrane tethering mediated by their cognate Rab GTPase, Rab11a, in a GTP-dependent manner (Figs. 7, 8. 10, and 11). This finding leads us to hypothesize that cytoskeletal motor proteins, including class V myosins and also microtubule-based motor proteins, act as tethering factors (not "tethers") that directly and positively regulate Rab-mediated membrane tethering (37, 51). A more detailed understanding of the protein machinery of Rab-mediated membrane tethering will require further studies using a chemically defined reconstitution system, which may focus on testing tethering by heterotypic Rab combinations, on determining the specific regions in Rab molecules responsible for tethering, and on reconstituting Rab-mediated tethering in the presence of different types of Rab effectors.

Experimental procedures

Protein expression and purification

The coding sequences for the eight isoforms of Rab-family GTPases (Rab1a, Rab3a, Rab4a, Rab5a, Rab7a, Rab9a, Rab11a, and Rab14) in humans and for human HRas GTPase were amplified by PCR with Human Universal QUICK-Clone cDNA II (Clontech, Mountain View, CA) as a template cDNA and KOD-Plus-Neo DNA polymerase (Toyobo, Osaka, Japan) as described (18). The amplified PCR fragments contained the sequence encoding a human rhinovirus (HRV) 3C protease site (Leu-Glu-Val-Leu-Phe-Gln-Gly-Pro) upstream of the initial ATG codons and the sequence encoding polyhistidine residues (His_{12}) downstream of the codons for a C-terminal residue, yielding the full-length Rab and HRas proteins with three extra N-terminal residues (Gly-Pro-Gly) and a C-terminal His_{12} tag after HRV 3C protease cleavage. For Rab11a, the PCR fragment without the polyhistidine-coding sequence was also amplified as described above, to prepare the Rab11a protein lacking the C-terminal His_{12} tag (untagged Rab11a). All of these PCR fragments for the Rab-family and HRas GTPases were inserted into a pET-41 Ek/LIC vector (Novagen, Madison, WI), which is designed to express an N-terminal GST-His_6–tagged protein, using the ligation-independent cloning method (Novagen).

Recombinant Rab and HRas proteins were expressed in the *Escherichia coli* BL21(DE3) cells (Novagen) harboring the pET-41-based vectors in lysogeny broth (LB) medium (1 liter each) with kanamycin (50 μg/ml) by induction with 0.1 mM IPTG at 37 °C for 3 h. *E. coli* cells harvested after IPTG induction were resuspended in 40 ml each of RB150 (20 mM Hepes-NaOH, pH 7.4, 150 mM NaCl, 10% glycerol) containing 0.1 mM GTP, 5 mM $MgCl_2$, 1 mM DTT, 1 mM PMSF, and 1.0 μg/ml pepstatin A, freeze-thawed in liquid nitrogen followed by a water bath at 30 °C, lysed by sonication using a UD-201 ultrasonic disrupter (Tomy Seiko, Tokyo, Japan), and then ultracentrifuged at 50,000 rpm for 75 min at 4 °C with a 70 Ti rotor (Beckman Coulter, Indianapolis, IN). The supernatants obtained were mixed with COSMOGEL GST-Accept beads (50% slurry, 4 ml each; Nacalai Tesque, Kyoto, Japan) and incubated at 4 °C for 2 h with gentle agitation to isolate GST-His_6-tagged Rab-His_{12} and HRas-His_{12} proteins. The protein-bound GST-Accept beads were washed four times in RB150 containing 5 mM $MgCl_2$ and 1 mM DTT (8 ml each), resuspended in the same buffer (4 ml each) supplemented with HRV 3C protease (4 units/ml final, Novagen), and incubated without agitation (4 °C, 16 h) to cleave off and elute Rab-His_{12} and HRas-His_{12} proteins. After centrifugation of the bead suspensions (15,300 × *g*, 10 min, 4 °C), the purified Rab-His_{12} and HRas-His_{12} proteins were harvested from the supernatants.

For class V myosins, the coding sequences of the globular tail domains of human myosin 5a (Myo5A-GTD, residues 1534–1855) and myosin 5b (Myo5B-GTD, residues 1526–1848) with the sequence encoding a HRV 3C–protease site upstream of the initial codons were amplified by PCR as described above and then cloned into a pET-30 Ek/LIC vector (Novagen) expressing an N-terminal His_6-tagged protein. Recombinant Myo5A-GTD(1534–1855) and Myo5B-GTD(1526–1848) proteins were expressed in the *E. coli* BL21(DE3) cells harboring the pET-30–based vectors in LB medium with kanamycin (1 liter each) by induction with 0.1 mM IPTG (16 °C, 16 h). *E. coli* cells were resuspended in 40 ml each of RB150 containing $MgCl_2$ (5 mM), DTT (1 mM), PMSF (1 mM), and pepstatin A (1.0 μg/ml) followed by freeze-thaw treatment, sonication, and ultracentrifugation as described above. The supernatants were mixed with Complete His-tag purification resin beads (50% slurry, 4 ml each; Hoffmann-la Roche) and incubated at 4 °C for 2 h with

Figure 11. Rab11a- and Myo5-GTD–dependent membrane tethering requires the membrane attachment of Rab11a on both of two opposing membranes destined to tether. *A*, schematic representation of the streptavidin bead–based liposome-tethering assay described in *B* and *C* using two types of liposomes bearing either biotin-PE/DOGS-NTA/Rh-PE or FL-PE/DOGS-NTA and purified Rab11a-His_{12} and Myo5-GTD proteins. *B*, streptavidin bead–based liposome-tethering assays with Rab11a-His_{12} and Myo5-GTDs. The biotin-labeled and FL-labeled liposomes were incubated with streptavidin-coated magnetic beads (30 °C, 2 h), mixed with Rab11a-His_{12} and Myo5A-GTD or Myo5B-GTD, and incubated further (30 °C, 10 min). The FL-labeled liposomes tethered to the biotin-labeled liposomes on streptavidin beads were quantified by measuring the FL fluorescence. For a control, Rab11a, Myo5A-GTD, and Myo5B-GTD were omitted from the reactions where indicated (*lanes 1–4*). *AU*, arbitrary units. *C*, streptavidin bead–based liposome-tethering assays were employed with Rab11a-His_{12} and Myo5-GTDs as described in *B*, but FL-labeled liposomes lacking DOGS-NTA were used instead where indicated (*lanes 2* and *4*). *D–G*, fluorescence microscopy was performed as described in Fig. 7, *F–K*, with Rh-labeled liposomes (0.4 mM lipids), FL-labeled liposomes (0.4 mM lipids), Rab11a-His_{12} (3 μM), and Myo5A-GTD (*D* and *E*) or Myo5B-GTD (*F* and *G*) (each at 3 μM). Rh-labeled liposomes lacking DOGS-NTA were used instead where indicated (*E* and *G*). *Scale bars*: 10 μm.

gentle agitation to isolate His_6-tagged Myo5A-GTD and Myo5B-GTD proteins. The protein-bound beads were washed four times in RB150 containing 5 mM $MgCl_2$, 1 mM DTT, and 20 mM imidazole (8 ml each), resuspended in the same buffer (2 ml each) containing HRV 3C protease (15 units/ml, Novagen), and incubated with gentle agitation (4 °C, 16 h). After centrifugation of the bead suspensions (15,300 × *g*, 10 min, 4 °C), purified Myo5A-GTD and Myo5B-GTD proteins, which had been cleaved off from the beads, were harvested from the supernatants and dialyzed against RB150 containing 5 mM $MgCl_2$ and 1 mM DTT.

The protein concentrations of the purified Rab, HRas, and Myo5-GTD proteins were determined using Protein Assay CBB Solution (Nacalai Tesque) and BSA as a standard protein. These purified recombinant proteins were boiled (100 °C for 5 min) in 1.6% SDS and then analyzed by SDS-PAGE and Coomassie Blue staining.

GTPase activity assay

GTP hydrolysis activities of human Rab-family and HRas GTPases were assayed by quantitating released free phosphate molecules during the hydrolytic reactions using the malachite green-based reagent, BIOMOL Green (Enzo Life Sciences, Farmingdale, NY) as described (18, 52), with modifications. Purified recombinant Rab-family and HRas proteins (2 μM final) were incubated at 30 °C for 1 h in RB150 containing 6 mM $MgCl_2$, 1 mM DTT, and 1 mM GTP or GTPγS. After a 1-h incubation, the reaction mixtures (50 μl each) were supplemented with the BIOMOL Green reagent (50 μl each), further incubated at 30 °C for 30 min, and measured for absorbance at 620 nm in a clear 96-well microplate (Falcon 351172, Corning) using the SpectraMax Paradigm plate reader with an ABS-MONO cartridge (Molecular Devices, Sunnyvale, CA). All of the data obtained were corrected by subtracting the absorbance values of the control reactions without any Rab and HRas GTPases. To calculate the concentrations of released phosphate molecules in the reactions, phosphate standard samples (2.5–160 μM final, Enzo Life Sciences) were also incubated and assayed using the same protocol. Means and standard deviations of the specific GTPase activities for purified Rab-family and HRas proteins (μM phosphate/min/μM protein) were determined from three independent experiments.

Liposome preparation

All non-fluorescent lipids were purchased from Avanti Polar Lipids (Alabaster, AL). Fluorescent lipids Rh-PE and FL-PE were obtained from Molecular Probes (Eugene, OR). Lipid mixes for the Rh-labeled liposomes used in the liposome turbidity assays, fluorescence microscopy, and liposome co-sedimentation assays contained 1-palmitoyl-2-oleoyl-phosphatidylcholine (POPC, 42% (mol/mol)), 1-palmitoyl-2-oleoyl-PE (POPE, 16.5%), soy PI (10%), 1-palmitoyl-2-oleoyl-phosphatidylserine (POPS, 5%), cholesterol (20%), DOGS-NTA (6%), and Rh-PE (0.5%). For the biotin/Rh-labeled and FL-labeled liposomes used in streptavidin bead–based liposome-tethering assays and fluorescence microscopy, lipid mixes contained 1-palmitoyl-2-oleoyl-phosphatidylcholine (41%), 1-palmitoyl-2-oleoyl-PE (14.5% and 16.5% for the biotin/Rh-labeled and FL-labeled liposomes, respectively), soy PI (10%), 1-palmitoyl-2-oleoyl-phosphatidylserine (5%), cholesterol (20%), DOGS-NTA (6%), biotin-PE (2% for the biotin/Rh-labeled liposomes), and fluorescent lipids (1.5% of Rh-PE and FL-PE for the biotin/Rh-labeled and FL-labeled liposomes, respectively). Dried lipid films harboring these physiological mimic lipid compositions (18, 28) were completely resuspended in RB150 containing 5 mM $MgCl_2$ and 1 mM DTT by vortexing, yielding 8 mM total lipids final, and then incubated at 37 °C for 1 h with shaking, freeze-thawed in liquid N_2 and a water bath at 30 °C, and extruded 21 times through polycarbonate filters (pore diameter, 400 or 1000 nm; Avanti Polar Lipids) in a mini-extruder (Avanti Polar Lipids) at 40 °C. The lipid concentrations of the extruded liposomes were determined from the fluorescence of Rh-PE (λex = 550 nm, λem = 590 nm) and FL-PE (λex = 486 nm, λem = 529 nm) using a SpectraMax Paradigm plate reader with the TUNE cartridge (Molecular Devices) and a black 384-well plate (Corning 3676). Liposome solutions were diluted with RB150 containing 5 mM $MgCl_2$ and 1 mM DTT to 5 mM total lipids final and stored at 4 °C.

Liposome turbidity assay

Membrane tethering of Rab GTPase-anchored liposomes was monitored by the turbidity changes in the liposome solutions as described elsewhere (18, 25–27) with modifications. After preincubating the liposome suspensions and Rab protein solutions separately at 30 °C for 10 min, the liposomes (400 nm diameter, 0.5 mM total lipids final concentration) were mixed with Rab proteins (0.5–4.0 μM final concentration) in RB150 containing 5 mM $MgCl_2$ and 1 mM DTT (total 150 μl for each) immediately followed by measuring the absorbance changes of the liposome suspensions at 400 nm in a DU720 spectrophotometer (Beckman Coulter) at room temperature for 300 s. For the assays with class V myosins, Rab proteins (1 μM final) were preincubated at 30 °C for 30 min in the presence of Myo5A-GTD or Myo5B-GTD (0.5–2.0 μM final) before mixing with liposomes. All liposome turbidity data were obtained from one experiment and were typical of those from more than three independent experiments.

Liposome co-sedimentation assay

Rh-labeled liposome suspensions (400 nm diameter, 1 mM total lipids in final) were mixed with purified Rab, HRas, or BSA proteins (2 μM in final) in RB150 containing 5 mM $MgCl_2$ and 1 mM DTT (100 μl each) and subsequently incubated at 30 °C for 30 min. For the experiments with class V myosins, the reaction mixtures were further supplemented with GTP (1 mM final) and Myo5A-GTD or Myo5B-GTD (2 μM final). After incubation, these reactions were ultracentrifuged at 50,000 rpm for 30 min at 4 °C with a TLA100 rotor and an Optima TLX Ultracentrifuge (Beckman Coulter). The pellets and supernatants obtained were analyzed by SDS-PAGE and Coomassie Blue staining.

Fluorescence microscopy

After preincubating liposome suspensions and Rab protein solutions separately at 30 °C for 10 or 30 min, liposomes (1000 nm diameter, 0.5 or 0.8 mM total lipids in final) and Rab proteins (3.0 or 4.0 μM final) were mixed in RB150 containing 5 mM

$MgCl_2$ and 1 mM DTT (total 50 μl for each), further incubated at 30 °C for 30 min or 1 h, transferred to ice, and subjected to fluorescence microscopy. For the reactions with class V myosins, Rab11a-His_{12} (3 μM final) was preincubated in the presence of Myo5A-GTD or Myo5B-GTD (3 μM final) at 30 °C for 30 min before incubating with liposomes. A drop of the incubated reactions (5 μl each) was placed on a microscope slide (S2111, Matsunami Glass, Kishiwada, Japan) and covered with an 18-mm coverslip (Matsunami Glass). Fluorescence microscopy was performed using a BZ-9000 fluorescence microscope (Keyence, Osaka, Japan) equipped with Plan Apo 40X NA 0.95 and Plan Apo VC 100X NA 1.40 oil objective lenses (Nikon, Tokyo, Japan) and TRITC and GFP-BP filters (Keyence). The digital images obtained were processed using the BZ-II viewer application (Keyence) and ImageJ2 software (National Institutes of Health, Bethesda, MD). The particle sizes of the Rab-mediated liposome clusters were measured using ImageJ2 after setting the lower intensity threshold level to 100 and the upper intensity threshold level to 255 (19, 53).

Streptavidin bead–based liposome-tethering assay

A liposome-tethering assay using a streptavidin-coated bead was performed as described previously (18, 52) with modifications. The biotin/Rh-labeled liposomes (400 nm diameter, 0.08 mM lipids final) and FL-labeled liposomes (400 nm diameter, 0.2 mM lipids final) were incubated with streptavidin-coated magnetic beads (Dynabeads M-280 streptavidin, Invitrogen) at 30 °C for 2 h, supplemented with protein solutions containing Rab11a-His_{12} and Myo5A-GTD or Myo5B-GTD (3 μM each in final), which had been preincubated at 30 °C for 30 min, and further incubated at 30 °C for 10 min with gentle agitation. The liposome-bound streptavidin beads were washed twice with RB150 containing $MgCl_2$ (5 mM) and DTT (1 mM), resuspended in RB150 containing 100 mM octyl-β-glucoside by vortexing to completely solubilize the liposomes on beads, and centrifuged. To quantify the FL-labeled liposomes co-isolated with the beads, FL fluorescence (λ excitation = 495 nm, λ emission = 520 nm, emission cut-off = 515 nm) in the supernatants obtained was measured using a SpectraMAX Gemini XPS plate reader (Molecular Devices). Means and standard deviations of the FL fluorescence signals were determined from three independent experiments.

Author contributions—J. M. designed the research, and J. M. and M. I. performed the experiments. J. M. and M. I. analyzed the data, and J. M. wrote the manuscript.

Acknowledgments—We thank Dr. Naoki Tamura (Institute for Protein Research, Osaka University, now Fukushima Medical University School of Medicine) for valuable suggestions on this project and for substantial contributions toward preparing the expression vectors for human Rab GTPases. We are grateful to Drs. Junichi Takagi and Yukiko Matsunaga (Institute for Protein Research, Osaka University) for access to fluorescence microscopy experiments.

References

1. Bonifacino, J. S., and Glick, B. S. (2004) The mechanisms of vesicle budding and fusion. *Cell* **116,** 153–166
2. Jahn, R., and Scheller, R. H. (2006) SNAREs: Engines for membrane fusion. *Nat. Rev. Mol. Cell Biol.* **7,** 631–643
3. Baker, R. W., and Hughson, F. M. (2016) Chaperoning SNARE assembly and disassembly. *Nat. Rev. Mol. Cell Biol.* **17,** 465–479
4. Stenmark, H. (2009) Rab GTPases as coordinators of vesicle traffic. *Nat. Rev. Mol. Cell Biol.* **10,** 513–525
5. Hutagalung, A. H., and Novick, P. J. (2011) Role of Rab GTPases in membrane traffic and cell physiology. *Physiol. Rev.* **91,** 119–149
6. Grosshans, B. L., Ortiz, D., and Novick, P. (2006) Rabs and their effectors: Achieving specificity in membrane traffic. *Proc. Natl. Acad. Sci. U.S.A.* **103,** 11821–11827
7. Wandinger-Ness, A., and Zerial, M. (2014) Rab proteins and the compartmentalization of the endosomal system. *Cold Spring Harb. Perspect. Biol.* **6,** a022616
8. Waters, M. G., and Pfeffer, S. R. (1999) Membrane tethering in intracellular transport. *Curr. Opin. Cell Biol.* **11,** 453–459
9. Cai, H., Reinisch, K., and Ferro-Novick, S. (2007) Coats, tethers, Rabs, and SNAREs work together to mediate the intracellular destination of a transport vesicle. *Dev. Cell* **12,** 671–682
10. Yu, I. M., and Hughson, F. M. (2010) Tethering factors as organizers of intracellular vesicular traffic. *Annu. Rev. Cell Dev. Biol.* **26,** 137–156
11. Scales, S. J., Chen, Y. A., Yoo, B. Y., Patel, S. M., Doung, Y. C., and Scheller, R. H. (2000) SNAREs contribute to the specificity of membrane fusion. *Neuron* **26,** 457–464
12. McNew, J. A., Parlati, F., Fukuda, R., Johnston, R. J., Paz, K., Paumet, F., Söllner, T. H., and Rothman, J. E. (2000) Compartmental specificity of cellular membrane fusion encoded in SNARE proteins. *Nature* **407,** 153–159
13. Parlati, F., Varlamov, O., Paz, K., McNew, J. A., Hurtado, D., Söllner, T. H., and Rothman, J. E. (2002) Distinct SNARE complexes mediating membrane fusion in Golgi transport based on combinatorial specificity. *Proc. Natl. Acad. Sci. U.S.A.* **99,** 5424–5429
14. Izawa, R., Onoue, T., Furukawa, N., and Mima, J. (2012) Distinct contributions of vacuolar Qabc- and R-SNARE proteins to membrane fusion specificity. *J. Biol. Chem.* **287,** 3445–3453
15. Furukawa, N., and Mima, J. (2014) Multiple and distinct strategies of yeast SNAREs to confer the specificity of membrane fusion. *Sci. Rep.* **4,** 4277
16. Lo, S. Y., Brett, C. L., Plemel, R. L., Vignali, M., Fields, S., Gonen, T., and Merz, A. J. (2012) Intrinsic tethering activity of endosomal Rab proteins. *Nat. Struct. Mol. Biol.* **19,** 40–47
17. Brunet, S., and Sacher, M. (2014) Are all multisubunit tethering complexes bona fide tethers? *Traffic* **15,** 1282–1287
18. Tamura, N., and Mima, J. (2014) Membrane-anchored human Rab GTPases directly mediate membrane tethering *in vitro*. *Biol. Open* **3,** 1108–1115
19. Hickey, C. M., and Wickner, W. (2010) HOPS initiates vacuole docking by tethering membranes before trans-SNARE complex assembly. *Mol. Biol. Cell* **21,** 2297–2305
20. Ho, R., and Stroupe, C. (2015) The HOPS/class C Vps complex tethers membranes by binding to one Rab GTPase in each apposed membrane. *Mol. Biol. Cell* **26,** 2655–2663
21. Cheung, P. Y., Limouse, C., Mabuchi, H., and Pfeffer, S. R. (2015) Protein flexibility is required for vesicle tethering at the Golgi. *eLife* **4,** e12790
22. Ho, R., and Stroupe, C. (2016) The HOPS/class C Vps complex tethers high-curvature membranes via a direct protein-membrane interaction. *Traffic* **17,** 1078–1090
23. Murray, D. H., Jahnel, M., Lauer, J., Avellaneda, M. J., Brouilly, N., Cezanne, A., Morales-Navarrete, H., Perini, E. D., Ferguson, C., Lupas, A. N., Kalaidzidis, Y., Parton, R. G., Grill, S. W., and Zerial, M. (2016) An endosomal tether undergoes an entropic collapse to bring vesicles together. *Nature* **537,** 107–111
24. Rojas, A. M., Fuentes, G., Rausell, A., and Valencia, A. (2012) The Ras protein superfamily: Evolutionary tree and role of conserved amino acids. *J. Cell Biol.* **196,** 189–201
25. Ohki, S., Düzgüne, N., and Leonards, K. (1982) Phospholipid vesicle aggregation: Effect of monovalent and divalent ions. *Biochemistry* **21,** 2127–2133

26. Hui, E., Gaffaney, J. D., Wang, Z., Johnson, C. P., Evans, C. S., and Chapman, E. R. (2011) Mechanism and function of synaptotagmin-mediated membrane apposition. *Nat. Struct. Mol. Biol.* **18,** 813–821
27. Liu, T. Y., Bian, X., Romano, F. B., Shemesh, T., Rapoport, T. A., and Hu, J. (2015) Cis and trans interactions between atlastin molecules during membrane fusion. *Proc. Natl. Acad. Sci. U.S.A.* **112,** E1851–E1860
28. van Meer, G., Voelker, D. R., and Feigenson, G. W. (2008) Membrane lipids: Where they are and how they behave. *Nat. Rev. Mol. Cell Biol.* **9,** 112–124
29. Takamori, S., Holt, M., Stenius, K., Lemke, E. A., Grønborg, M., Riedel, D., Urlaub, H., Schenck, S., Brügger, B., Ringler, P., Müller, S. A., Rammner, B., Gräter, F., Hub, J. S., De Groot, B. L., *et al*. (2006) Molecular anatomy of a trafficking organelle. *Cell* **127,** 831–846
30. Nagle, J. F., and Tristram-Nagle, S. (2000) Structure of lipid bilayers. *Biochim. Biophys. Acta* **1469,** 159–195
31. Erickson, H. P. (2009) Size and shape of protein molecules at the nanometer level determined by sedimentation, gel filtration, and electron microscopy. *Biol. Proced. Online* **11,** 32–51
32. Khan, A. R., and Ménétrey, J. (2013) Structural biology of Arf and Rab GTPases' effector recruitment and specificity. *Structure* **21,** 1284–1297
33. Zhang, X. M., Ellis, S., Sriratana, A., Mitchell, C. A., and Rowe, T. (2004) Sec15 is an effector for the Rab11 GTPase in mammalian cells. *J. Biol. Chem.* **279,** 43027–43034
34. Wu, S., Mehta, S. Q., Pichaud, F., Bellen, H. J., and Quiocho, F. A. (2005) Sec15 interacts with Rab11 via a novel domain and affects Rab11 localization *in vivo*. *Nat. Struct. Mol. Biol.* **12,** 879–885
35. Wu, B., and Guo, W. (2015) The exocyst at a glance. *J. Cell Sci.* **128,** 2957–2964
36. Lapierre, L. A., Kumar, R., Hales, C. M., Navarre, J., Bhartur, S. G., Burnette, J. O., Provance, D. W., Jr, Mercer, J. A., Bähler, M., and Goldenring, J. R. (2001) Myosin Vb is associated with plasma membrane recycling systems. *Mol. Biol. Cell* **12,** 1843–1857
37. Hammer, J. A., 3rd, Wu, X. S. (2002) Rabs grab motors: defining the connections between Rab GTPases and motor proteins. *Curr. Opin. Cell Biol.* **14,** 69–75
38. Hammer, J. A., 3rd, Sellers, J. R. (2012) Walking to work: roles for class V myosins as cargo transporters. *Nat. Rev. Mol. Cell Biol.* **13,** 13–26
39. Lindsay, A. J., Jollivet, F., Horgan, C. P., Khan, A. R., Raposo, G., McCaffrey, M. W., and Goud, B. (2013) Identification and characterization of multiple novel Rab-myosin Va interactions. *Mol. Biol. Cell* **24,** 3420–3434
40. Roland, J. T., Bryant, D. M., Datta, A., Itzen, A., Mostov, K. E., and Goldenring, J. R. (2011) Rab GTPase-Myo5B complexes control membrane recycling and epithelial polarization. *Proc. Natl. Acad. Sci. U.S.A.* **108,** 2789–2794
41. Pylypenko, O., Attanda, W., Gauquelin, C., Lahmani, M., Coulibaly, D., Baron, B., Hoos, S., Titus, M. A., England, P., and Houdusse, A. M. (2013) Structural basis of myosin V Rab GTPase-dependent cargo recognition. *Proc. Natl. Acad. Sci. U.S.A.* **110,** 20443–20448
42. Pylypenko, O., Welz, T., Tittel, J., Kollmar, M., Chardon, F., Malherbe, G., Weiss, S., Michel, C. I., Samol-Wolf, A., Grasskamp, A. T., Hume, A., Goud, B., Baron, B., England, P., Titus, M. A., *et al*. (2016) Coordinated recruitment of Spir actin nucleators and myosin V motors to Rab11 vesicle membranes. *eLife* **5,** e17523
43. Donovan, K. W., and Bretscher, A. (2012) Myosin-V is activated by binding secretory cargo and released in coordination with Rab/exocyst function. *Dev. Cell* **23,** 769–781
44. Gerondopoulos, A., Langemeyer, L., Liang, J. R., Linford, A., and Barr, F. A. (2012) BLOC-3 mutated in Hermansky-Pudlak syndrome is a Rab32/38 guanine nucleotide exchange factor. *Curr. Biol.* **22,** 2135–2139
45. Blümer, J., Rey, J., Dehmelt, L., Mazel, T., Wu, Y. W., Bastiaens, P., Goody, R. S., and Itzen, A. (2013) RabGEFs are a major determinant for specific Rab membrane targeting. *J. Cell Biol.* **200,** 287–300
46. Cabrera, M., and Ungermann, C. (2013) Guanine nucleotide exchange factors (GEFs) have a critical but not exclusive role in organelle localization of Rab GTPases. *J. Biol. Chem.* **288,** 28704–28712
47. Chia, P. Z., and Gleeson, P. A. (2014) Membrane tethering. *F1000Prime Rep.* **6,** 74
48. Kuhlee, A., Raunser, S., and Ungermann, C. (2015) Functional homologies in vesicle tethering. *FEBS Lett.* **589,** 2487–2497
49. Pereira-Leal, J. B., and Seabra, M. C. (2000) The mammalian Rab family of small GTPases: definition of family and subfamily sequence motifs suggests a mechanism for functional specificity in the Ras superfamily. *J. Mol. Biol.* **301,** 1077–1087
50. Stein, M., Pilli, M., Bernauer, S., Habermann, B. H., Zerial, M., and Wade, R. C. (2012) The interaction properties of the human Rab GTPase family: Comparative analysis reveals determinants of molecular binding selectivity. *PLoS ONE* **7,** e34870
51. Akhmanova, A., and Hammer, J. A., 3rd. (2010) Linking molecular motors to membrane cargo. *Curr. Opin. Cell Biol.* **22,** 479–487
52. Sugiura, S., and Mima, J. (2016) Physiological lipid composition is vital for homotypic ER membrane fusion mediated by the dynamin-related GTPase Sey1p. *Sci. Rep.* **6,** 20407
53. Stroupe, C., Hickey, C. M., Mima, J., Burfeind, A. S., and Wickner, W. (2009) Minimal membrane docking requirements revealed by reconstitution of Rab GTPase-dependent membrane fusion from purified components. *Proc. Natl. Acad. Sci. U.S.A.* **106,** 17626–17633